MODELING ULTRASONIC FIELDS IN COMPLEX GEOMETRIES

A PROJECT REPORT

submitted by

ADARSH K.

in partial fulfillment of the requirements
for the award of the degrees of

BACHELOR OF TECHNOLOGY and MASTER OF TECHNOLOGY

in

MECHANICAL ENGINEERING

under the guidance of

PROF. KRISHNAN BALASUBRAMANIAM

DEPARTMENT OF MECHANICAL ENGINEERING
INDIAN INSTITUTE OF TECHNOLOGY MADRAS
CHENNAI-600036
APRIL 2005

CERTIFICATE

This is to certify that the thesis titled **'Modeling Ultrasonic Fields in Complex Geometries'** submitted by **Adarsh K** to the Indian Institute of Technology, Madras in partial fulfillment of the requirements for the award of the degrees of Bachelor of Technology and Master of Technology is a bona fide record of work done by him under the supervision of Prof. Krishnan Balasubramaniam. The contents of this thesis, in full or in parts, have not been submitted to any other Institute or University for the award of any degree or diploma.

Dr S Srinivasa Murthy
(Head of Department)
Department of Mechanical Engineering
Indian Institute of Technology Madras

Dr Krishnan Balasubramaniam
(Guide)
Department of Mechanical Engineering
Indian Institute of Technology Madras

Chennai – 600036
May 5, 2005

TABLE OF CONTENTS

ACKNOWLEDGEMENTS

I express my heartfelt thanks and gratitude to my guide and mentor, Dr. Krishnan Balasubramaniam, for supporting me right from my freshman year at IIT. He has been responsible for providing me with many fabulous opportunities that have helped me shape my career. His ability to provide practical ideas and to improvise on any given situation has always been a great source of inspiration for me.

I am grateful to Dr. C.V. Krishnamurthy for sharing his knowledge and experience so freely. This work would not be possible without his timely support and valuable insights. I am also grateful to Soumya for helping me in performing the experiments and in fabricating the experimental setup.

My personal thanks to my friends Subramanian, Radha, Ram, Bharat, Sethuraman and Padma Kumar for their interest and support throughout my sojourn at IIT. I will always cherish those memorable hours I spent working with them. I also take this opportunity to thank the members of CNDE (Center for Non Destructive Evaluation) for their support, comradeship and help without which this work could not have been done.

This project would not have been possible if it had not been for my parents' immutable support for every endeavor of mine. My brother, an alumnus of IIT, has been a great source of inspiration for all my accomplishments.

My profound gratitude to the almighty, without His blessings, I would have been nowhere.

ABSTRACT

Ultrasonic Non-Destructive Testing (NDT) is a widely used testing method that is commonly employed in estimating the integrity of several engineering specimens. By definition, an ultrasonic simulation model uses physical equations and numerical methods to predict the result of an experiment. Because it is a software model, any parameter that effects the results can be changed or varied as needed. One important motivation for using such models is the relatively low cost of software predictions compared to the cost of comparable experiments. The simulation of ultrasonic testing using appropriate models allows to perform parametric studies and to obtain quantitative simulated results.

An important part of any ultrasonic simulation is the computation of the ultrasonic field within the component. Any generic model used for this purpose should take care of two important aspects - Geometry modeling and Transducer modeling. Geometry modeling is required to model a test specimen accurately. The usual method adopted is to model the specimen in a CAD or Solid Modeling software and then use it for simulating ultrasonic fields inside the specimen. There are several analytical and numerical methods to model ultrasonic transducers. One such method is the point source superposition technique or the patch model, which allows including all aspects relevant to testing simulation as far as bulk wave propagation is concerned.

The main objective of this project is to develop a generic 3-D ultrasonic simulation package that includes geometry as well as transducer modeling to evaluate the ultrasonic fields inside the test specimen. A visualization package to visualize the test part as well as the ultrasonic fields using Ray tracing has been developed. The software also

includes solid modeling features to model the solid geometry of the test specimen. It also supports import of surface mesh files from meshing software like ANSYS or HYPERMESH. A novel hybrid method combining ray tracing and the patch model is used to calculate the ultrasonic fields inside the test specimen.

Simulation studies were done on a flat block to verify the validity of the ray-tracing model. The studies were done on Flat Bottom Holes and in Pipes with EDM notches. A-Scans were generated for different orientation of the transducer. B-Scans were also generated in the case of the Flat Bottom Hole. The results obtained were found to be consistent with expected results.

Simulation and experiments were done to design inspection methods for testing very thin pipes. Initial studies were done to assess the feasibility of the inspection of such pipes by using ray tracing. The studies were done to find the standoff distance as well as the angle of inspection that is optimum for inspection. It was found that the transducer position was critical in getting a proper response. Based on the initial optimization studies, an experimental setup was built to validate the results experimentally. The B-Scan images obtained showed good correlation both with the arrival time of the signal as well as the amplitudes of the signals. Certain key features were noted both in experiments as well as in simulations. The results obtained from experiments confirmed the validity of the simulations.

LIST OF FIGURES

NOMENCLATURE

c_L	Longitudinal Wave velocity
c_S	Shear Wave velocity
f	Frequency
k	Wave Number
u	Displacement
C	Elastic Constant
E	Young's Modulus
Z	Acoustic Impedence
α	Attenuation Factor
γ	Half Divergence Angle of the Beam
θ	Incident Angle
λ	Wavelength
ν	Frequency
ρ	Density
σ	Stress
τ	Shear stress
ψ	Wave Potential
ω	Frequency

CHAPTER 1

INTRODUCTION TO ULTRASONIC TESTING

1.1 ULTRASONICS

Ultrasonics is a branch of acoustics dealing with the generation and use of (generally) inaudible acoustic waves. There are two broad areas of use, sometimes called as the low- and high-intensity applications. In low-intensity applications, the intent is to convey information about or through a system, while in high-intensity applications, the intent is to permanently alter a system. To some extent, the low and high-intensity fields are also delineated by a frequency range and power level. Thus, low-intensity applications typically involve frequencies about 10 MHz or higher and power levels approximately milliwatts. High intensity applications will typically involve frequencies of 5 to 100 kHz and powers of hundreds to thousands of watts. In fact, the total frequency range of all ultrasonic applications is enormous, ranging from 5-10 kHz to as high as 10 GHz. There are also applications, such as sonar, which are exceptions to the previous categorizations, since intense power levels are involved in conveying information via underwater sound.

Ultrasonic materials characterization is the most important application of ultrasonics in aerospace engineering and engineering mechanics. Historically, ultrasonic nondestructive testing (NDT) has been used almost exclusively for detecting macroscopic discontinuities in structures after they have been in service for some time. It has become increasingly evident that it is practical and cost effective to expand the role of ultrasonic NDT testing to include all aspects of materials production and application. Research efforts are being directed at developing and perfecting NDT capable of monitoring material production processes, material integrity following transport, storage and fabrication and the amount and rate of degradation during service. In addition, efforts are underway to develop techniques capable of quantitative discontinuity sizing, permitting determination of material response using fracture mechanics analysis, as well as techniques for quantitative materials characterization to replace the qualitative techniques used in the past. Ultrasonic techniques play a prominent role in these developments because they afford useful and versatile methods for evaluating microstructures, associated mechanical properties, as well as detecting microscopic and macroscopic discontinuities in solid materials.

1.2 ULTRASONIC TESTING

Ultrasonic Testing uses high frequency sound energy to conduct examinations and make measurements. Ultrasonic inspection can be used for flaw detection, evaluation, dimensional measurements and material characterization. A typical UT inspection system consists of several functional units, such as the pulser/receiver, transducer and display devices. A pulser/receiver is an electronic device that can produce high voltage electrical pulse. Driven by the pulser, the transducer generates high frequency ultrasonic energy. The sound energy propagates through the materials in the form of waves. When there is a discontinuity (such as a crack) in the wave path, part of the energy will be reflected back from the flaw surface. The reflected wave signal is transformed into electrical signal by the transducer and is displayed on a screen. The reflected signal strength is displayed versus the time from signal generation to when an echo was received. Signal travel time can be directly related to the distance that the signal traveled. From the signal, information about the reflector location, size, orientation and other features can sometimes be gained.

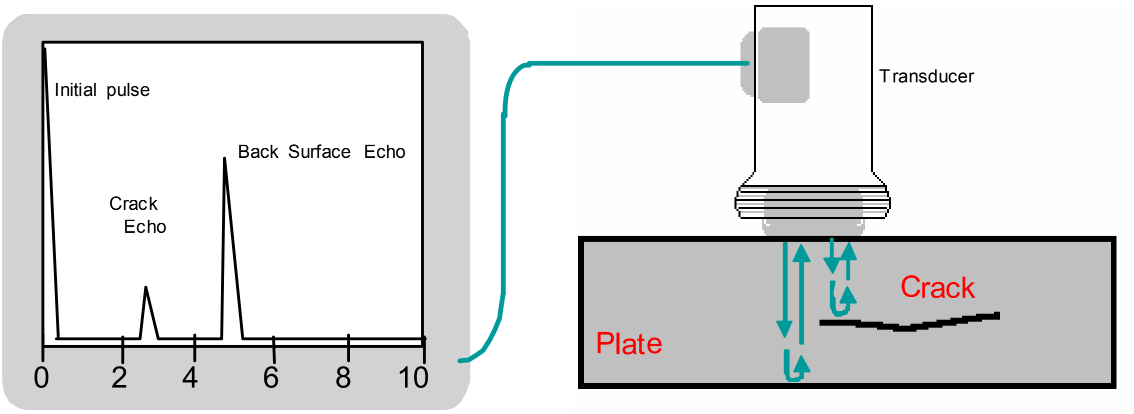

Figure 1.1: Ultrasonic Testing System

Ultrasonic Inspection is a very useful and versatile NDT (Non Destructive Testing) method. Some of the advantages of ultrasonic inspection that are often cited include

- It is sensitive to both surface and subsurface discontinuities.
- The depth of penetration for flaw detection or measurement is superior to other NDT methods.
- Only single-sided access is needed when the pulse-echo technique is used.
- It is high accuracy in determining reflector position and estimating size and shape.
- Minimal part preparation required.
- Electronic equipment provides instantaneous results.
- Detailed images can be produced with automated systems.
- It has other uses such as thickness measurements, in addition to flaw detection.

As with all NDT methods, ultrasonic inspection also has its limitations, which include

- Surface must be accessible to transmit ultrasound.
- Skill and training is more extensive than with some other methods.

- It normally requires a coupling medium to promote transfer of sound energy into test specimen.
- Materials that are rough, irregular in shape, very small, exceptionally thin or not homogeneous are difficult to inspect.
- Cast iron and other coarse-grained materials are difficult to inspect due to low sound transmission and high signal noise.
- Linear defects oriented parallel to the sound beam may go undetected.
- Reference standards are required for both equipment calibration, and characterization of flaws.

The above introduction introduces the NDT method of ultrasonic testing. However, to perform an inspection effectively using ultrasonics, much more about the method needs to be known. These include knowledge of the science involved in ultrasonic inspection, the equipment that is commonly used, some of the measurement techniques used, as well as other information.

1.3 WAVE PROPAGATION

Ultrasonic testing is based on time-varying deformations or vibrations in materials, which is generally referred to as acoustics. All material substances are comprised of atoms, which may be forced into vibrational motion about their equilibrium positions. Many different patterns of vibrational motion exist at the atomic level. However, most are irrelevant to acoustics and ultrasonic testing. Acoustics is focused on particles that contain many atoms that move in unison to produce a mechanical wave. When a material is not stressed in tension or compression beyond its elastic limit, its individual particles perform elastic oscillations. When the particles of a medium are displaced from their equilibrium positions, internal (electrostatic) restoration forces arise. It is these elastic restoring forces between particles, combined with inertia of the particles, which leads to oscillatory motions of the medium.

In solids, sound waves can propagate in four principle modes that are based on the way the particles oscillate. Sound can propagate as longitudinal waves, shear waves, surface waves, and in thin materials as plate waves. Longitudinal and shear waves are the two modes of propagation most widely used in ultrasonic testing. The particle movement responsible for the propagation of longitudinal and shear waves is shown in Figure 1.2.

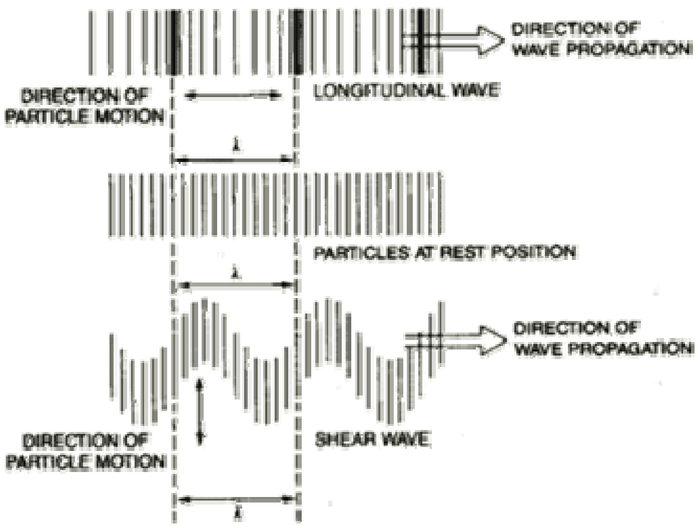

Figure 1.2: Longitudinal and Shear Waves

In longitudinal waves, the oscillations occur in the longitudinal direction or the direction of wave propagation. Since compressional and dilatational forces are active in these waves, they are also called pressure or compressional waves. They are also sometimes called density waves because their particle density fluctuates as they move. Compression waves can be generated in liquids, as well as solids because the energy travels through the atomic structure by a series of comparison and expansion (rarefaction) movements. In the transverse or shear wave, the particles oscillate at a right angle or transverse to the direction of propagation. Shear waves require an acoustically solid material for effective propagation. Therefore, they are not effectively propagated in liquids or gasses and are relatively weak when compared to longitudinal waves.

Solid molecules can support vibrations in other directions. Hence, a number of different types (modes) of sound waves are possible. As mentioned previously, longitudinal and transverse (shear) waves are most often used in ultrasonic inspection. However, at surfaces and interfaces, various types of elliptical or complex vibrations of the particles make other waves possible. Some of these wave modes such as Raleigh and Lamb waves are also useful for ultrasonic inspection.

Surface or Raleigh waves travel the surface of a relative thick solid material penetrating to a depth of one wavelength. The particle movement has an elliptical orbit as shown in the image and animation below. Raleigh waves are useful because they are very sensitive to surface defects and since they will follow the surface around, curves can be used to inspect areas that other waves might have difficulty reaching.

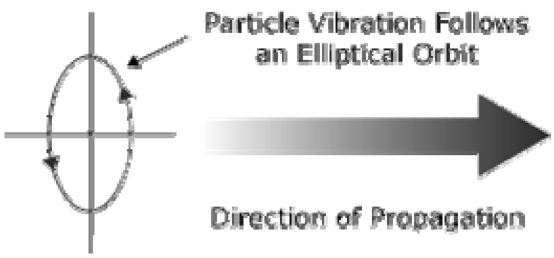

Figure 1.3: Raleigh Waves

Plate waves can be propagated only in very thin metals. Lamb waves are the most commonly used plate waves in NDT. Lamb waves are a complex vibrational wave that travels through the entire thickness of a material. Propagation of Lamb waves depends on density, elastic, and material properties of a component, and they are influenced by a great deal by selected frequency and material thickness. With Lamb waves, a number of modes of particle vibration are possible, but the two most common are symmetrical and asymmetrical. The complex motion of the particles is similar to the elliptical orbits for surface waves.

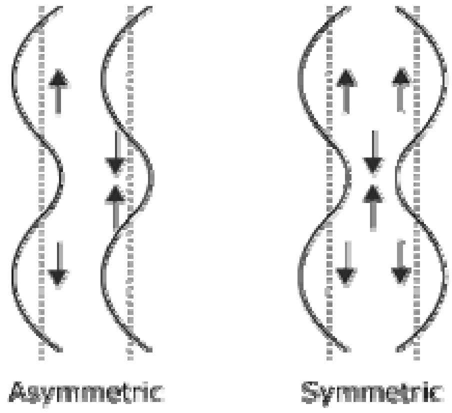

Figure 1.4: Lamb Wave Modes

Table 1.1 summarizes many, but not all, of the wave modes possible in solids.

Wave Type in Solids	**Particle Vibrations**
Longitudinal	Parallel to wave direction
Transverse (Shear)	Perpendicular to wave direction
Surface - Raleigh	Elliptical orbit - symmetrical mode
Plate Wave - Lamb	Component perpendicular to surface (extensional wave)
Plate Wave - Love	Parallel to plane layer, perpendicular to wave direction
Stoneley	Wave guided along interface
Sezawa	Anti-symmetric mode

Table 1.1: Wave Modes in Solids

1.4 PROPERTIES OF ACOUSTIC PLANE WAVES

Among the properties of waves propagating in isotropic solid materials are wavelength, frequency, and velocity. The wavelength is directly proportional to the velocity of the wave and inversely proportional to the frequency of the wave. This relationship is shown in Equation(1.1).

$$\lambda = \frac{c}{f} \tag{1.1}$$

As can be noted from Equation(1.1), a change in frequency will result in a change in wavelength. In ultrasonic testing, the shorter wavelength resulting from an increase in frequency will usually provide for the detection of smaller discontinuities. The wavelength of the ultrasound used has significant affect on the probability of detecting a discontinuity. A rule of thumb in industrial inspections is that discontinuities that are larger than one-half the size of wavelength can be usually be detected.

Sensitivity and resolution are two terms that are often used in ultrasonic inspection to describe a technique's ability to locate flaws. Sensitivity is the ability to locate small discontinuities. Sensitivity generally increases with higher frequency (shorter wavelengths). Resolution is the ability of the system to locate discontinuities that are close together within the material or located near the part surface. Resolution also generally increases as the frequency increases.

The wave frequency can also affect the capability of an inspection in adverse ways. Therefore, selecting the optimal inspection frequency often involves maintaining a balance between favorable and unfavorable results of the selection. Before selecting an inspection frequency, the grain structure, material thickness, size, type and probable location of the discontinuity should be considered. As frequency increases, sound tends to scatter from large or course grain structure and from small imperfections within a material. Cast materials often have coarse grains and other sound scatters that require lower frequencies to be used for evaluations of these products. Wrought and forged products with directional and refined grain structure can usually be inspected with higher frequency transducers.

Since more things in a material are likely to scatter a portion of the sound energy at higher frequencies, the penetrating power (or the maximum depth in a material that flaws can be located) is also reduced. Frequency also has an effect on the shape of the ultrasonic beam. Beam spread, or the divergence of the beam from the center axis of the transducer, and how it is affected by frequency will be discussed later. It should be mentioned that a number of other variables would also affect the ability of ultrasound to locate defects. These include pulse length, type and voltage applied to the crystal, properties of the crystal, backing material, transducer diameter and the receiver circuitry of the instrument.

1.5 ACOUSTIC VELOCITY IN SOLIDS

Sound travels at different speeds in different materials. The general relationship between the speed of sound in a solid and its density and elastic constants is given by Equation(1.2). Here C is the elastic constant, c is the speed of sound and ρ is the material density.

$$c = \sqrt{\frac{C_{ij}}{\rho}} \tag{1.2}$$

This equation may take a number of different forms depending on the type of wave (longitudinal or shear) and which of the elastic constants that are used. The typical elastic constants of materials include

- Young's Modulus, **E**: a proportionality constant between uniaxial stress and strain
- Poisson's Ratio, **ν**: the ratio of radial strain to axial strain
- Bulk modulus, **K**: a measure of the incompressibility of a body subjected to hydrostatic pressure
- Shear Modulus, **G**: also called rigidity, a measure of substance's resistance to shear
- Lame's Constants, **λ** and **μ**: material constants that are derived from Young's Modulus and Poisson's Ratio

When calculating the velocity of a longitudinal wave, Young's Modulus and Poisson's Ratio are commonly used. When calculating the velocity of a shear wave, the shear modulus is used. It is often most convenient to make the calculations using Lame's Constants, which are derived from Young's Modulus and Poisson's Ratio.

It must also be mentioned that the subscript ij attached to C in the above equation is used to indicate the directionality of the elastic constants with respect to the wave type and direction of wave travel. In isotropic materials, the elastic constants are the same for all directions within the material. However, most materials are anisotropic and the elastic constants differ with each direction. For example, in a piece of rolled aluminum plate, the grains are elongated in one direction and compressed in the others and the elastic constants for the longitudinal direction are different than those for the transverse or short transverse directions.

1.6 ACOUSTIC IMPEDANCE

Sound travels through materials under the influence of sound pressure. Because molecules or atoms of a solid are bound elastically to one another, the excess pressure results in a wave propagating through the solid. The acoustic impedance (Z) of a material is defined as the product of density (ρ) and acoustic velocity (c) of that material.

$$Z = \rho c \tag{1.3}$$

Acoustic impedance is important in several calculations. Some of them include

- Determining acoustic transmission and reflection at the boundary of two materials having different acoustic impedance
- Designing ultrasonic transducers
- Assessing absorption of sound in a medium

1.7 SNELL'S LAW

When an ultrasound wave passes through an interface between two materials at an oblique angle, and the materials have different indices of refraction, it produces both reflected and refracted waves. This also occurs with light and this makes objects you see across an interface appear to be shifted relative to where they really are. Refraction takes place at an interface due to the different velocities of the acoustic waves within the two materials. The velocity of sound in each material is determined by the material properties (elastic modules and density) for that material. In Figure 1.5 below, a series of plane waves are shown traveling in one material and entering a second material that has a higher acoustic velocity. Therefore, when the wave encounters the interface between these two materials, the portion of the wave in the second material is moving faster than the portion of the wave in the first material. It can be seen that this causes the wave to bend.

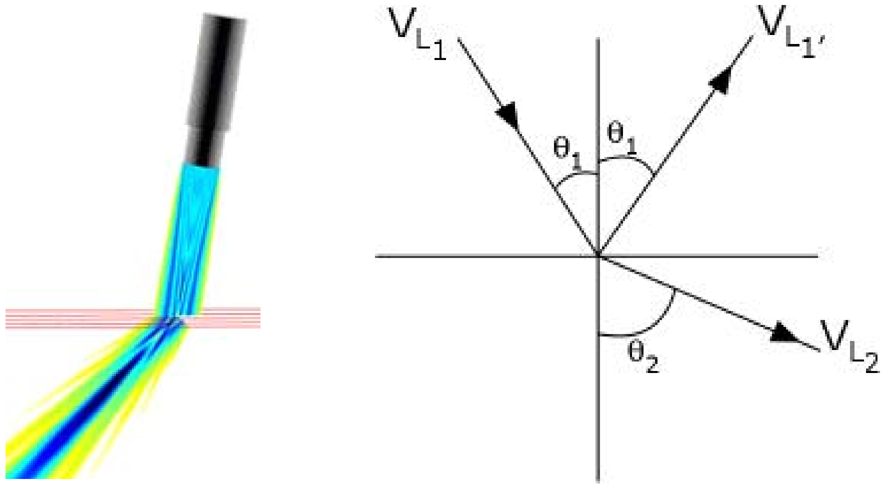

Figure 1.5: Refraction of Sound Waves

Snell's Law describes the relationship between the angles and the velocities of the waves. Snell's law equates the ratio of material velocities c_1 and c_2 to the ratio of the sine's of incident (θ_1) and refraction (θ_2) angles, as shown in Equation(1.4).

$$\frac{\sin(\theta_1)}{c_1} = \frac{\sin(\theta_2)}{c_2} \tag{1.4}$$

When a longitudinal wave moves from a slower to a faster material, a particular incident angle makes the angle of refraction for the wave 90°. This is known as the first critical angle. The first critical angle can be found from Snell's law by putting in an angle of 90° for the angle of the refracted ray. At the critical angle of incidence, much of the acoustic energy is in the form of an inhomogeneous compression wave, which travels along the interface and decays exponentially with depth from the interface. This wave is sometimes referred to as a "creep wave." Because of there inhomogeneous nature and the fact that they decay rapidly, creep waves are not used as extensively as Raleigh surface waves in NDT. However, creep waves are sometimes useful because they suffer less from surface irregularities and coarse material microstructure, due to their longer wavelengths, than Raleigh waves.

1.8 MODE CONVERSION

When sound travels in a solid material, one form of wave energy can be transformed into another form. For example, when a longitudinal wave hits an interface at an angle, some of the energy can cause particle movement in the transverse direction to start a shear (transverse) wave. Mode conversion, occurs when a wave encounters an interface between materials of different acoustic impedance and the incident angle is not normal to the interface. Since mode conversion occurs every time a wave encountered interface at an angle, ultrasonic signals can become confusing at times.

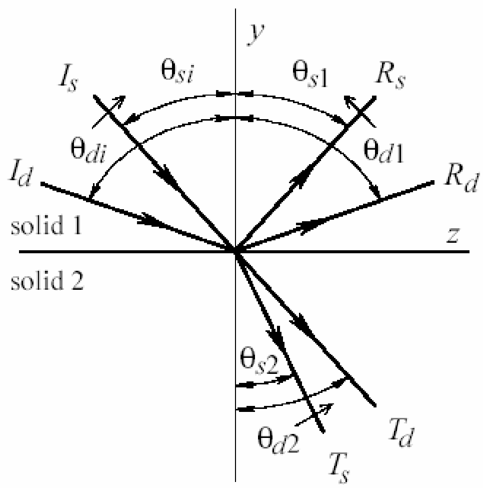

Figure 1.6: Solid-Solid Interface

Beyond the first critical angle, only the shear wave propagates down into the material. For this reason, angle beam transducers use a shear wave so that the signal is not complicated by having two waves present. In many cases, there is also another incident angle that makes the angle of refraction for the shear wave 90 degrees. This is know as the second critical angle and at this point, all of the wave energy is reflected or refracted into a surface following shear wave or shear creep wave. Slightly beyond the second critical angle, surface waves will be generated.

The generalized Snell's law gives the angle of the reflected and refracted rays, is given by Equation(1.5).

$$\frac{\sin(\theta_{di})}{c_{d1}} = \frac{\sin(\theta_{si})}{c_{s1}} = \frac{\sin(\theta_{d1})}{c_{d1}} = \frac{\sin(\theta_{s1})}{c_{s1}} = \frac{\sin(\theta_{d2})}{c_{d2}} = \frac{\sin(\theta_{s2})}{c_{s2}} \tag{1.5}$$

1.9 Reflection and Transmission Coefficients

The particle displacement amplitudes of the incident, reflected, and transmitted longitudinal waves are I_d, T_d and R_d, respectively. Similarly, the particle displacement amplitudes of the incident, reflected, and transmitted shear waves are I_s, T_s and R_s. Only two stress components are relevant to the boundary conditions.

$$\tau_{yy} = \lambda \frac{\delta u_z}{\delta z} + (\lambda + 2\mu)\frac{\delta u_y}{\delta y} \tag{1.6}$$

$$\tau_{zy} = \mu\left(\frac{\delta u_y}{\delta z} + \frac{\delta u_z}{\delta y}\right) \tag{1.7}$$

$$\begin{aligned} \mu_1 &= \rho_1 c_{s1}^2 \\ \lambda_1 + 2\mu_1 &= \rho_1 c_{d1}^2 \\ \mu_2 &= \rho_2 c_{s2}^2 \\ \lambda_2 + 2\mu_2 &= \rho_2 c_{d2}^2 \end{aligned} \tag{1.8}$$

The boundary conditions require that both normal and transverse velocity and stress components be continuous at the interface, where the incident wave can be either longitudinal (I_d= 1, I_s = 0) or shear (I_s = 1, I_s = 0).

$$\begin{bmatrix} -u_y^{d1} & +u_y^{d2} & -u_y^{s1} & +u_y^{s2} \\ -u_z^{d1} & +u_z^{d2} & -u_z^{s1} & +u_z^{s2} \\ -\tau_{yy}^{d1} & +\tau_{yy}^{d2} & -\tau_{yy}^{s1} & +\tau_{yy}^{s2} \\ -\tau_{zy}^{d1} & +\tau_{zy}^{d2} & -\tau_{zy}^{s2} & +\tau_{zy}^{s2} \end{bmatrix} = \begin{bmatrix} u_y^i \\ u_z^i \\ \tau_{yy}^i \\ \tau_{zy}^i \end{bmatrix} \tag{1.9}$$

This can be written as Equation(1.10) depending on whether longitudinal or shear wave incidence is considered.

$$\begin{bmatrix} a_{11} & a_{12} & a_{13} & a_{14} \\ a_{21} & a_{22} & a_{23} & a_{24} \\ a_{31} & a_{32} & a_{33} & a_{34} \\ a_{41} & a_{42} & a_{43} & a_{44} \end{bmatrix} \begin{bmatrix} R_d \\ T_d \\ R_s \\ T_s \end{bmatrix} = \begin{bmatrix} b_1 \\ b_2 \\ b_3 \\ b_4 \end{bmatrix} or \begin{bmatrix} c_1 \\ c_2 \\ c_3 \\ c_4 \end{bmatrix} \tag{1.10}$$

The matrix elements A_{ij}, B_i and C_i can be easily calculated from simple geometrical considerations.

$$A=\begin{bmatrix} -\cos\theta_{d1} & -\cos\theta_{d2} & -\sin\theta_{s1} & \sin\theta_{s2} \\ -\sin\theta_{d1} & \sin\theta_{d2} & \cos\theta_{s1} & \cos\theta_{s2} \\ -Z_{d1}\cos 2\theta_{s1} & Z_{d2}\cos 2\theta_{s2} & -Z_{s1}\sin 2\theta_{s1} & -Z_{s2}\sin 2\theta_{s2} \\ -Z_{s1}\dfrac{c_{s1}}{c_{d1}}\sin 2\theta_{d1} & -Z_{s2}\dfrac{c_{s2}}{c_{d2}}\sin 2\theta_{d2} & Z_{s1}\sin 2\theta_{s1} & -Z_{s2}\sin 2\theta_{s2} \end{bmatrix} \tag{1.11}$$

For brevity, the common ($-i\omega$) factor was omitted in the last two rows. (The sign of all elements in the third column of matrix **A** has been changed with respect to Auld's [3] to account for the opposite polarization of the reflected shear wave in his book.)

$$B=\begin{bmatrix} -\cos\theta_{di} \\ \sin\theta_{di} \\ Z_{d1}\cos 2\theta_{di} \\ -Z_{s1}\dfrac{c_{s1}}{c_{d1}}\sin 2\theta_{di} \end{bmatrix} \textit{and } C=\begin{bmatrix} \sin\theta_{si} \\ \cos\theta_{si} \\ -Z_{s1}\sin 2\theta_{si} \\ -Z_{s1}\cos 2\theta_{si} \end{bmatrix} \tag{1.12}$$

The reflection and transmission coefficients can be determined by applying the well-known Cramer's rule.

Figure 1.7 shows the schematic diagrams of reflection and transmission of waves for various combinations of materials.

In these figures and in the following, the first index of the reflection and transmission coefficients indicate the type of the incident wave. For example, R_{sd} is the dilatational reflection coefficient for shear wave incidence and T_{dd} is the dilatational transmission coefficient for dilatational wave incidence.

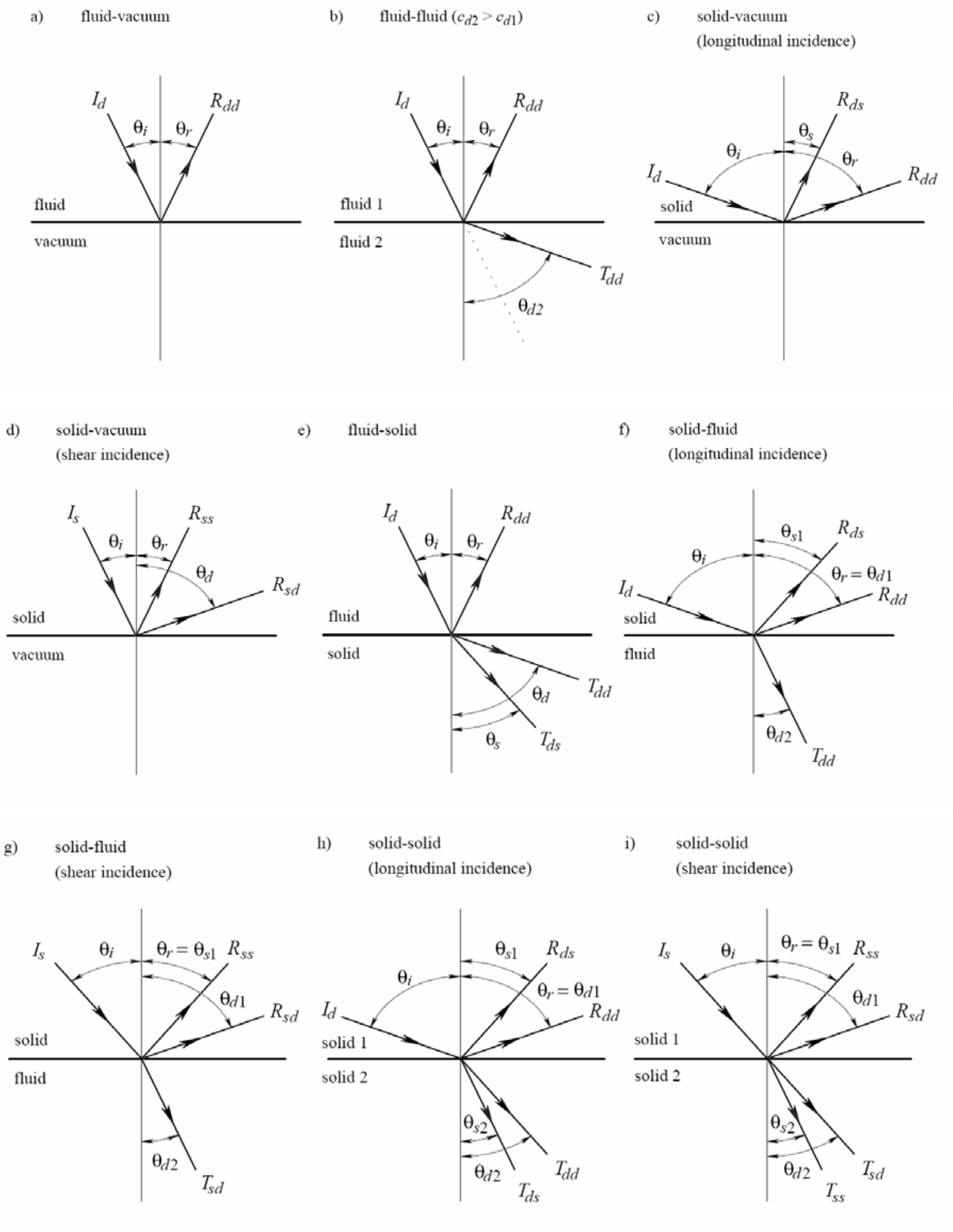

Figure 1.7: Reflection and Transmission Coefficients for different cases

1.10 Power Coefficient

The reflection and transmission coefficients determined from the above equations denote displacement ratios (without explicitly indicating it). In many cases, it is necessary to express the relative strength of the reflected and transmitted waves in terms of stress, intensity or power. The stress coefficients can be obtained from the corresponding displacement coefficients by accounting for the impedance differences.

$$\Gamma_{\alpha\beta}^{(stress)} = \Gamma_{\alpha\beta}^{(displacement)} \frac{Z_{\beta j}}{Z_{\alpha 1}} \tag{1.13}$$

Γ stands for either R (j = 1) or T (j = 2), and α and β are either d or s. For propagating modes, the intensity coefficients then can be easily calculated as a product of the corresponding displacement and stress coefficients.

$$\Gamma_{\alpha\beta}^{(intensity)} = \Gamma_{\alpha\beta}^{(displacement)} \Gamma_{\alpha\beta}^{(stress)} \tag{1.14}$$

Finally, for propagating modes the power coefficients can be obtained from the corresponding intensity coefficients by accounting for the different refraction angles.

$$\Gamma_{\alpha\beta}^{(power)} = \Gamma_{\alpha\beta}^{(displacement)} \Gamma_{\alpha\beta}^{(displacement)} \frac{Z_{\beta j}}{Z_{\alpha 1}} \frac{\cos\theta_{\beta j}}{\cos\theta_{\alpha 1}} \tag{1.15}$$

It should be mentioned that the power coefficients are identically zero for evanescent waves, which do not carry energy away from the interface.

The law of energy conservation can be written as given in Equation(1.16). It can be noted that the total energy at each interface is conserved and there is no loss at the interface.

$$R_{\alpha d}^{(power)} + R_{\alpha S}^{(power)} + T_{\alpha d}^{(power)} + T_{\alpha S}^{(power)} = 1 \qquad (1.16)$$

CHAPTER 2

ULTRASONIC SIMULATIONS

2.1 POTENTIAL USES OF MODELS

By definition, an ultrasonic simulation model uses physical equations and numerical methods to predict the result of an experiment. Because it is a software model, any parameter that effects the results can be changed or varied as needed. One important motivation for using such models is the relatively low cost of software predictions compared to the cost of comparable experiments.

The potential uses of the model fall into three basic categories.

- Can ultrasound reach the region of interest?
- What are the properties of the field in a region of interest?
- What is the response from the incident field on a given flaw?

The measurement model, in combination with some intelligent control software can answer even more queries that are complex. The control software can loop through a range of parameters to find optimum values for the inspection.

The models can be used to predict various physical parameters that are of interest in ultrasonic testing of any component. These include parameters like amplitude as a function of distance away from the transducer, amplitude loss when coupling into a particular material, beam focusing as it passes through a concave interface, beam bending as it mode converts and the beam spread as it propagates through the material.

Other parameters, which are also of interest, include information about the shape of the beam, phase curvature at a particular point, focal point, if any, in the region and presence of any regions of reduced amplitude in the inspection zone.

Flaw interaction models can predict the response from the incident field on a given flaw and the time-domain waveform response for a particular flaw. They can also predict the change of the flaw response change with probe orientation.

Another important use of simulations is that they cam be used for optimization studies. Some of the example optimization studies include

- Best location to place a probe to catch the signal
- Optimum wedge angle to maximize flaw response
- Optimum transducer to guarantee coverage
- Width of the region 3 dB's down from the peak response
- Best coverage that can be achieved with this transducer configuration, assuming infinitely small scan spacing
- Widest scan spacing that meets the scan quality objectives

To predict scan coverage it is essential to use a beam model since the fields of transducers have complex shapes that vary as a function of the interface and position in the part being inspected. The details of these shapes cannot be predicted via simple ray theories. An engineer is often interested in the relative beam widths at each location but current industry practice is to measure the beam width experimentally. In addition, one of the last steps in the design of a typical automated inspection is to measure the spot size and use it as a scan step, but if the beam width is measured after the system is assembled, it is apparent that little room for optimization is available.

By using simulations as a forward model to evaluate scan quality, an engineer in industry could see the quantitative effect of each parameter without performing an experiment and before buying the equipment. The scans that are refined by this software and then verified in the lab are likely to be much higher quality than typical inspections that are designed by rules of thumb and highly simplified analysis.

2.2 DIFFERENT TYPES OF MODELS

An important part of any ultrasonic simulation is the computation of the ultrasonic field within the component. Two different classes of approaches are currently developed in ultrasonic field modeling - numerical methods and analytical solutions. Numerical methods (finite elements, finite differences) can deal with almost arbitrary configurations but are limited by the long and often prohibitive computation time they take. For computer efficiency, they are generally limited to two-dimensional cases. Conversely, apart from a few exact solutions for a small range of simple geometries, analytic solutions in general include approximations, which must be experimentally validated. Analytic models can be efficiently implemented numerically and lead to short computation times, compatible with an intensive use. Therefore, practical simulators require such faster methods for computing the ultrasonic field produced by a given probe.

Much research has been focused on deriving an approximation of the exact expression in order to reduce the computational effort, to gain some physical insight into the problem, plane wave approximations [4] or a high frequency approximation [5] may be used. Exact analytical expressions have been derived for a number of nonmoving sources, for example, a point source [6], a line segment source, a circular source, an annular source or a rectangular source.

The exact expression for a finite source of normal traction is in general obtained as a spatial superposition of the elementary waves emitted by the point sources that may be thought to form the finite source. A direct numerical evaluation of the resulting double integral over the source surface has two major drawbacks. It offers no direct insight into the nature of the wave field; how properties like the directivity depend on the source parameters or the material parameters. Moreover, the numerical evaluation may be time consuming. This is especially the case when relatively high frequencies are involved, as the discretization of the spatial integrals is linked to the time sampling, which must be relatively fine in view of Shannon's sampling theorem.

2.3 RAY TRACING

Ray tracing uses the idea that sound waves propagate along straight line. Ignoring the wave/particle duality of sound waves, they are considered to be little particles (phonons) bouncing off objects and flying around. Each phonon on has a wavelength and energy (mode and intensity). After each bounce, some energy is lost until the phonon is absorbed. This phenomenon can essentially be modeled using rays. Rays can be used to know how the phonons interact with the objects.

For long-range sound propagation simulations, ray tracing has many advantages as well as drawbacks. Some of the advantages ray tracing offers is 3-D implementation with present-day computers and the capability of propagating only the acoustic field that will contribute to a single early arrival. Well-known drawbacks to ray tracing computations are the neglect of diffraction effects, infinite-amplitude results at caustics, and the often-quoted high-frequency approximation. However, other simulation techniques have advantages and drawbacks as well, suggesting the community should use many of the available propagation techniques and build strong conclusions through assimilation of results.

2.4 COMPARISON OF COMMERCIAL RAY TRACING MODELS

UTSim is an ultrasonic modeling package developed at CNDE, Iowa State University. It allows the user to simulate an inspection based on a solid CAD model. The code can generate fast approximations of ultrasound with ray tracing and beam models. The analysis is three-dimensional, user-friendly, with visual and numerical output. Its applications include Predicting where ultrasound will go in complex geometry, predicting the signal from a flaw inside the geometry, optimizing transducer locations and generating scan plans

To use the software system, a user first reads in the CAD part and the software automatically creates the voxel data structure. Second, all of the probe, flaw and material parameters are set by the user. Third, the scan region and initial spacing parameters are set based on the parametric CAD surfaces. The user then presses the button on the graphic user interface to start the scan. The software moves the transducer to the first location in the scan plan. The transducer shoots out a central ray to intersect the geometry. At the point of intersection, the surface properties are calculated. The surface properties and material properties are used to set up the boundary conditions for the beam model. The voxelizer sends all of the points near the central ray to the measurement model. For each voxel point, the measurement model positions the flaw at the point and calculates a time domain waveform. The peak-to-peak amplitudes of the waveforms are stored back in the voxelizer data structure. Figure 2.1 shows a screenshot of the software.

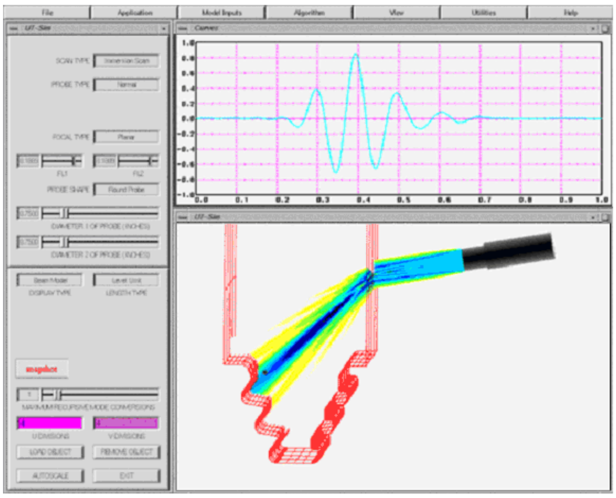

Figure 2.1: UTSim Software

3D ray tracing add-on module for AutoCAD 2000/2002 is a commercially available software module. This add-on module for AutoCAD computes and displays 3D ray tracing in components. A user can quickly visualize and adjust ultrasonic beam paths that include reflections, transmissions and mode conversions, within simple or complex geometries.

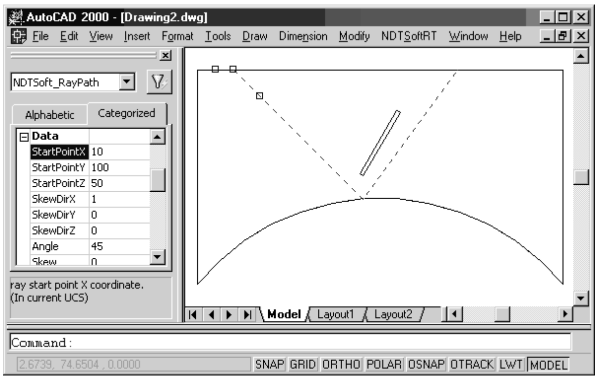

Figure 2.2: 3D Ray Tracing Add-on Module for AutoCAD

The ray tracing operates on solid model entities within AutoCAD, which are used to represent volumes of material of solid, liquid or gaseous state, depending on the properties that are set by the user. This program is totally integrated into AutoCAD. However, the ideas of transducers and energy coupling are not implanted. Hence, the program is essentially a conventional ray-tracing algorithm with the additional features of material properties and mode conversion.

RAYTRAIM, a product of AEA Technology is a program capable of simulating ultrasonic propagation. The domain itself is, however, restricted to a collection of bounded planes. The major difference between RAYTRAIM and other software is its capability to address anisotropic materials. It uses the standard ray tracing techniques. There is some kind of energy coupling but the method used is not mentioned. By the fact that the program is restricted to plane surfaces implies the possibility of beam models. The program also incorporates weld modeling (especially austenitic welds due to their inherent anisotropy). The program provides the interface for entering the planes that define the domain. Post-processing software is also provided to interpret the data that is obtained.

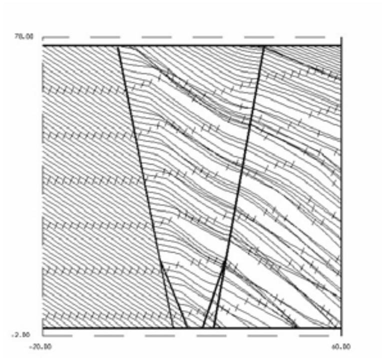

Figure 2.3: Raytraim

Imagine3D is the ultrasonic simulation software from UTEX scientific instruments. It is complete ultrasonic simulation software, which can be used for generating complete A-Scans and B-Scans. It can be used to model transducers of various kinds and operate them in different modes. It also generates RF data from the original output. The program uses ray tracing with no mention of beam modeling. Energy coupling has been used but the method is not disclosed. The inspection object can be created in a special modeling platform where a few primitives are available to build on. The major difference between this software and others (including ours) is the number of options for simulating the transducer. Beam focusing is also an option.

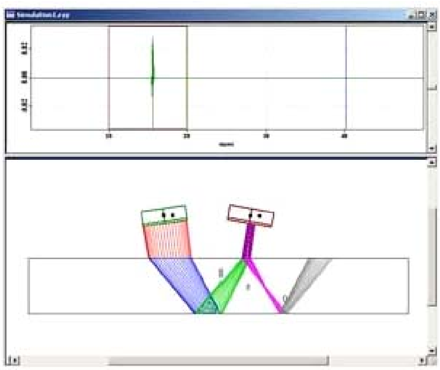

Figure 2.4: Imagine 3D

Table 2.1 lists the salient features of all the commercially available software. True geometric profile implies whether the complete geometry of the object is taken in to account for the simulation or approximations around the central ray are considered. Beam/Flaw models are completely theoretical methods of representing the flaws and the beam and involve complete mathematical formulation. It can be concluded from the table that no single software has the capability to model the physics of ultrasonic wave propagation completely in the presence of a complex geometry. This work is aimed at providing a comprehensive model that can account for complex geometry as well as the physics of ultrasonics.

	UTSim	**NDTSoft**	**RAYTRAIM**	**Imagine3D**
Owner	CNDE, Iowa	NDTSoft	AEA Tech.	UTEX Instruments
Platform	Independent	AutoCAD	Independent	Independent
Energy Modeling	☑	☒	☑	☑
True Geometry	☒	☑	☒	☑
Beam / Flaw Model	☑	☒	☒	☒
Anisotropy	☒	☒	☑	☒

Table 2.1: Comparison of Ultrasonic Ray Tracing Software

2.5 POINT SOURCE SUPERPOSITION TECHNIQUE

The point source superposition technique or the patch model is a conceptually simple scheme to evaluate the transducer fields in a homogenous medium at a single frequency [8]. It is understood that the RF waveforms in a pulsed experiment are to be obtained from many single frequency calculations and applying FFT routines. The model regards the transducer as made up of rectangular patch elements and invokes the superposition principle to evaluate the total transducer field from individual patch element fields. Figure 2.5 depicts the schematic of the patch model. The field at P is a superposition of the far-field contributions from all the patches. The far-field radiation pattern from each patch such as S is the well-known sinc function.

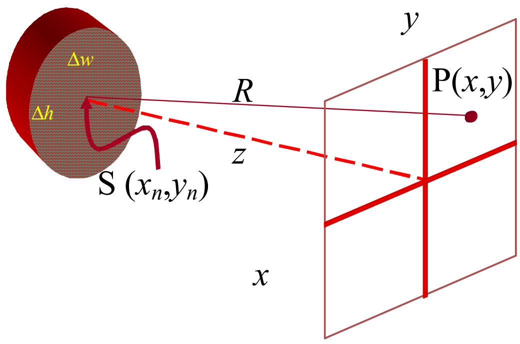

Figure 2.5: Point Source Superposition Technique

The key feature of the model is that the patch element dimensions are chosen such that the field point is in the far field of the element. Since the far-field radiation pattern of a rectangular aperture is well known and analytically expressible, the task of evaluating the complete transducer field is computationally simple. Consequently, as the field point moves farther from the transducer, the element dimensions increase and the number of elements eventually reduces to one as is to be expected. The total field from the transducer can be expressed as given in Equation(2.1).

$$p_0 = \frac{i\rho c \Delta A}{\lambda} \sum_{n=1}^{N} \frac{u_n}{\mathrm{R}} \mathrm{e}^{(-\alpha + ik)R} \,\mathrm{sinc}\, \frac{k(x_n - x)\Delta w}{2R} \,\mathrm{sinc}\, \frac{k(y_n - y)\Delta h}{2R} \qquad (2.1)$$

$$\mathrm{sinc}\, A = \frac{\sin \pi A}{\pi A} \qquad (2.2)$$

The elemental dimensions, Δw and Δh are chosen such that $z >> (\Delta w)^2 / 4\lambda$ and $z >> (\Delta h)^2 / 4\lambda$. In practice, a number F is chosen such that the condition in Equation(2.3) is satisfied.

$$\Delta w \leq \sqrt{\frac{4\lambda z}{F}} \tag{2.3}$$

A similar procedure is adopted for Δh. Fields from a planar circular transducer in a single homogeneous medium have been computed using the patch model and verified through implementation of two alternate methods of evaluating the transducer fields numerically both in the near-field and in the far-field [7].

CHAPTER 3

RAY TRACING

3.1 INTRODUCTION

An ultrasonic beam model is a combination of algebraic equations and numerical methods that solve a boundary value problem using the wave equation. In this case, the ultrasonic beam is modeled as a collection of rays. Thus, the rays are the fundamental units, which interact with the solid body and the surroundings. Once the rays are generated they are propagated as independent entities and do not interact with other rays.

Each ray is characterized by the position of its head, which is given by the global X, Y and Z coordinates. The ray also has three direction cosines that describe the direction in which the ray propagates. Each ray is also characterized by its type (whether shear or longitudinal) and its energy. The ray also has information about the amount of time lapsed from the time of its origin from the transducer.

The rays are produced as a radially symmetric or as a uniform beam by a transducer. The rays are equally distributed spatially based on the number of rays in the radial as well as the circumferential direction in the case of radially symmetric beam. In case of a uniform beam, the rays are equally distributed spatially in the X and Y directions. The two kinds of rays are shown in Figure 3.1.

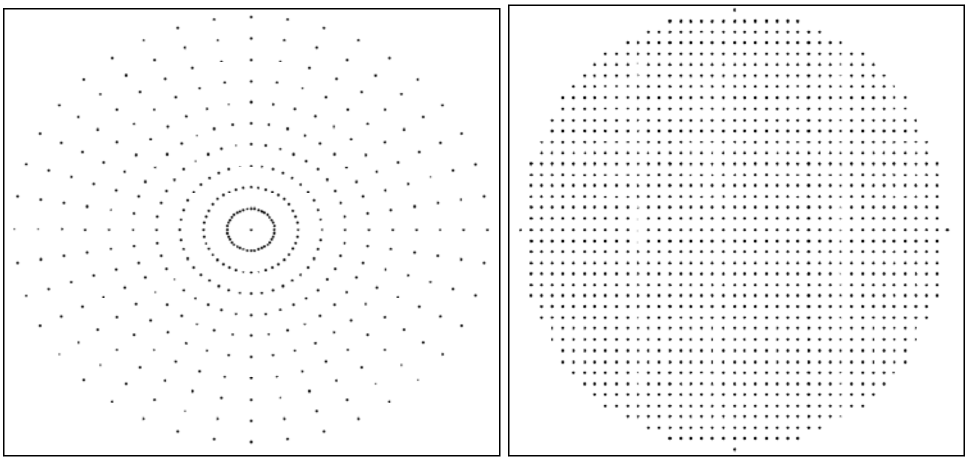

Figure 3.1: Radially Symmetric and Uniform Beam

Further, the rays are created as parallel, converging or diverging beams. This is shown in Figure 3.2.

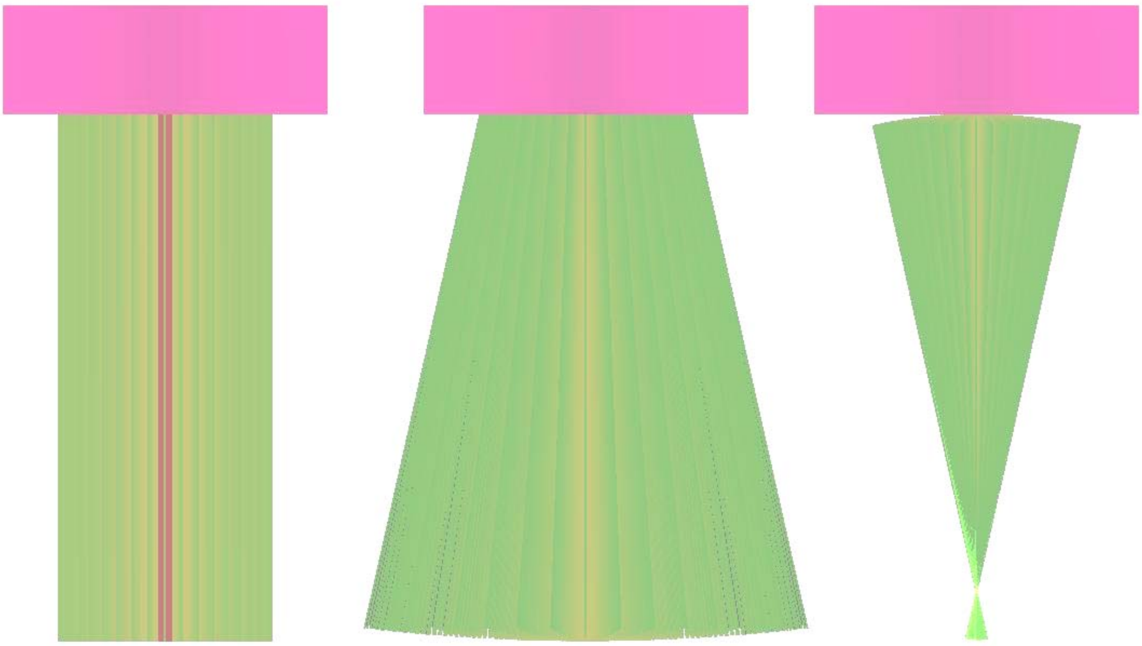

Figure 3.2: Cylindrical, Diverging and Converging Beams

3.2 GAUSSIAN ENERGY DISTRIBUTION

The rays are modeled as a Gaussian beam for the preliminary calculations based on ray tracing alone. A Cumulative Gaussian Distribution is used to distribute the energy spatially. The general formula for the probability density function of the normal distribution is given by Equation(3.1).

$$f(x) = \frac{e^{\frac{-(x-\mu)^2}{2\sigma^2}}}{\sigma\sqrt{2\pi}} \tag{3.1}$$

μ is called the location parameter and σ is called the scale parameter. The case where μ=0 and σ = 1 is called the standard normal distribution.

$$f(x) = \frac{e^{\frac{-x^2}{2}}}{\sqrt{2\pi}} \tag{3.2}$$

A probability distribution is characterized by location and scale parameters. Location and scale parameters are typically used in modeling applications. For example, Figure 3.2 is the probability density function for the standard normal distribution, which has the location parameter equal to zero and scale parameter equal to one.

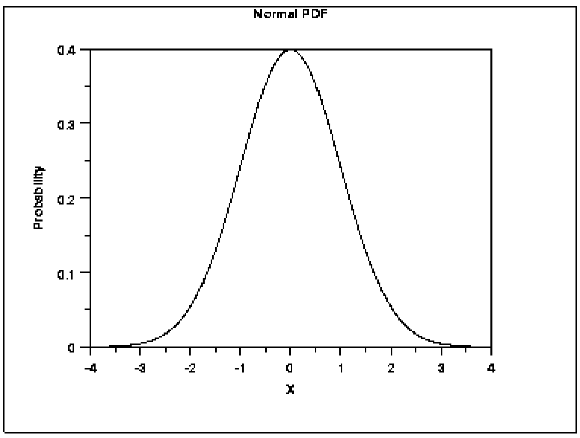

Figure 3.3: Standard Normal Distribution

Figure 3.4 shows the probability density function for a normal distribution with a location parameter of 10 and a scale parameter of 1.

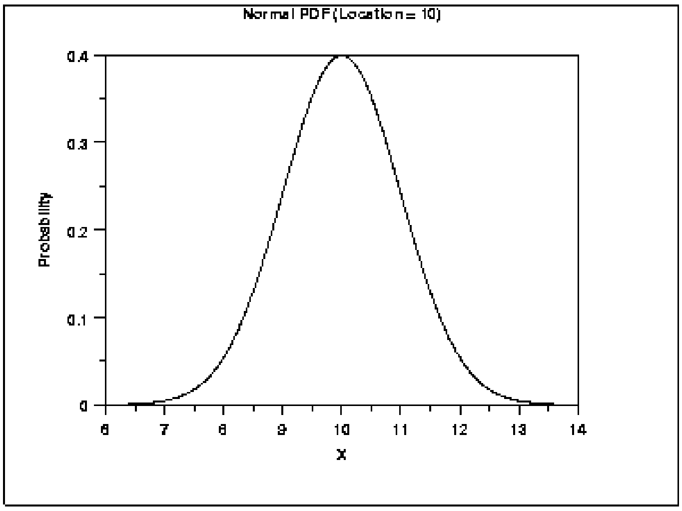

Figure 3.4: Shifted Normal Distribution Function

The effect of the location parameter is to translate the graph, relative to the standard normal distribution, 10 units to the right on the horizontal axis. A location parameter of -10 would have shifted the graph 10 units to the left on the horizontal axis. That is, a location parameter simply shifts the graph left or right on the horizontal axis.

The effect of a scale parameter greater than one is to stretch the probability density function. The effect of a scale parameter less than one is to compress the probability density function. The compressing approaches a spike as the scale parameter goes to zero. The cumulative normal distribution is used to find the area under the probability density function and this value is given to the rays of a particular discretized frequency.

The spatial distribution of the energy is done by using a normal distribution with radial distance as parameter. This energy is symmetric about the axis direction as the transducer is axis symmetric. Thus, the central ray has the maximum energy and the energy drops as distance from the center increase.

3.3 RAY CREATION

Vector algebra is used to find the direction of the rays originating from the transducer. Based on the standoff distance of the transducer from the surface of the specimen either diverging beam or a cylindrical beam is produced. If a focused transducer is used then a focused beam is produced.

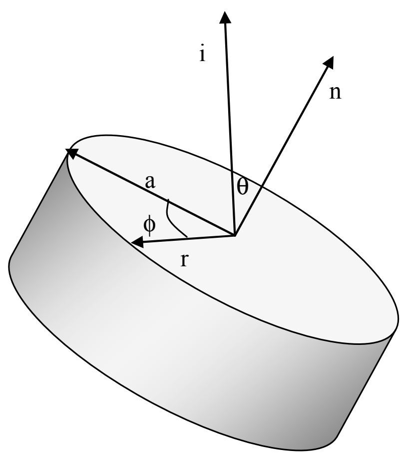

Figure 3.5: Ray Creation

$$
\begin{gathered}
\hat{a} = \alpha_1\ \hat{r} + \gamma_1\ (\hat{n} \times \hat{r}) \\
\text{Taking dot product with } \hat{r} \\
\cos\varphi = \alpha_1 \\
\hat{a} \cdot \hat{a} = 1 \Rightarrow \gamma_1 = \sin\varphi \\
\hat{a} = \cos\varphi\ \hat{r} + \sin\varphi\ (\hat{n} \times \hat{r}) \\
\hat{i} = \alpha\ \hat{a} + \beta\ \hat{n} \\
\hat{i} \cdot \hat{n} = \cos\theta \Rightarrow \beta = \cos\theta \\
\Rightarrow \alpha = \sin\theta
\end{gathered}
\tag{3.3}
$$

From the above derivation, we can find the direction vector for any ray at any specified angle from the normal and the reference direction. Thus, the direction vector is given by Equation(3.4).

$$(\sin\theta \ \cos\varphi)\hat{r} + (\sin\theta \ \sin\varphi)\ (\hat{n}\times\hat{r}) + (\cos\theta)\hat{n} \tag{3.4}$$

Here ***n*** is the normal to the transducer and ***r*** is the reference unit vector in the direction perpendicular to ***n***. The rays are created at the apparent origin and their origin is shifted along their direction of propagation to start from the face of the transducer. For cylindrical rays, the ray origin is shifted along the vector based on the distance required from the center of the transducer. The direction of the ray is same as the normal to the transducer.

3.4 Diverging Rays

An apparent beam origin is considered for the generation of a diverging beam of rays. All rays are considered to be originating from a point behind the transducer. To find the apparent beam origin, the near field distance of the transducer was also considered. The near field distance of the transducer in a given medium is given by Equation(3.5).

$$N = \frac{D^2 - \lambda^2}{4\lambda} \tag{3.5}$$

In Equation(3.5), D is the diameter of the transducer and λ is the wavelength of the wave.

This value changes depending upon the medium in which the transducer operates. The half angle of divergence (γ) is calculated from Equation(3.6) for different dB drops.

$$\sin\gamma = K_{dB} \times \frac{\lambda}{D} \tag{3.6}$$

where K_{dB} = 0.37 for 3dB drop

0.70 for 6dB drop

0.87 for 20dB drop

In the current case the 6dB drop is taken as standard and the values were calculated accordingly.

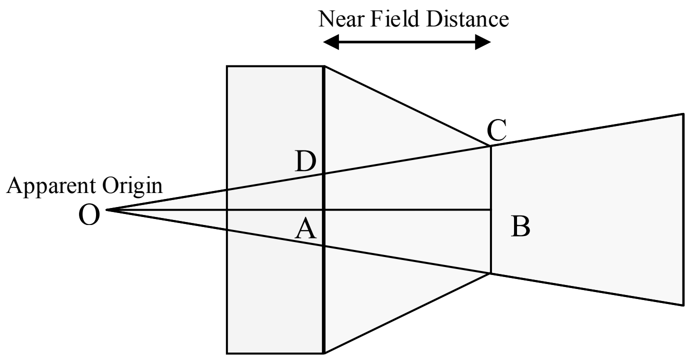

Figure 3.6: Beam Divergence

The apparent origin distance OA from the center of the transducer is given by Equation(3.7).

$$\begin{aligned} OA &= OB - AB \\ &= BC \cot\gamma - AB \\ &= \frac{D^2 - \lambda^2}{4\lambda} - \frac{D}{2}\frac{\sqrt{D^2 - K_{dB}^2\lambda^2}}{K_{dB}\lambda} \end{aligned} \tag{3.7}$$

3.5 GEOMETRICAL INTERFACE

The ray is propagated until it meets an interface. Once a ray meets an interface, new reflected and refracted rays are created based on the type of interface and the angle of incidence of the rays. Mode conversion also occurs at the interface. In the most general case (a solid-solid interface with incident angle below the first critical angle), four new rays are formed. These are the shear reflected and refracted rays and the longitudinal reflected and refracted rays. The incident ray can be either a shear ray or a longitudinal ray. Using the generalized Snell's law given in Equation(1.5) and the law of reflection and refraction (Incident ray, reflected ray or transmitted ray and the normal at the point of contact lie in the same plane), the vectors of the reflected and refracted ray are calculated.

The vector corresponding to the reflected ray is calculated based on whether the reflected ray is of the same mode as the incident ray or not. If the incident ray and reflected ray are of the same type then the reflected ray exists for all incidence angles. If the unit vector corresponding to the incident ray is denoted by ***i*** and the one corresponding to the normal by ***n***, the reflected ray ***r*** is given by Equation(3.8).

$$\hat{r} = 2(-\hat{i}\bullet\hat{n})\,\hat{n} + \hat{i} \tag{3.8}$$

If the reflected ray is of a different type, then the reflected ray is produced only if the incident angle is less than the critical angle for the two modes. This can be checked by the condition given in Equation(3.9).

$$1+\left(\frac{c_2}{c_1}\right)^2\left((-\hat{i}\bullet\hat{n})^2-1\right)>0 \tag{3.9}$$

In Equation(3.9), c1 is the velocity of the incident ray and c2 is the velocity of the mode converted reflected ray. Thus the vector equation of the reflected ray, if it is produced, is given by Equation(3.10).

$$\hat{r} = \left(\frac{c_2}{c_1}\right)\hat{i} + \left[\left(\frac{c_2}{c_1}\right)(-\hat{i}\bullet\hat{n}) \pm \sqrt{1+\left(\frac{c_2}{c_1}\right)^2\left((-\hat{i}\bullet\hat{n})^2-1\right)}\right]\hat{n} \tag{3.10}$$

The refracted ray is also calculated based on the same vector equations. The refracted ray exists only if the incident ray is less than the critical angle of incidence corresponding to the mode that is formed after refraction.

The condition for refracted ray to exist is the same as that of reflected ray i.e. Equation(3.9). The vector equation of the refracted ray is also given by Equation(3.10) but the normal used for calculations points in the same direction as the incident ray.

3.6 RAY TRACING ALGORITHM

Figure 3.7 gives the overall algorithm for ray tracing. The rays are initially created based on the requirement as Cylindrical, Diverging etc. as discussed previously in this chapter.

Figure 3.8 gives the ray-tracing algorithm for a single ray. The most important part of this algorithm is to find the intersection point of the ray with the objects present in the simulation. This is discussed in a greater detail in the next chapter.

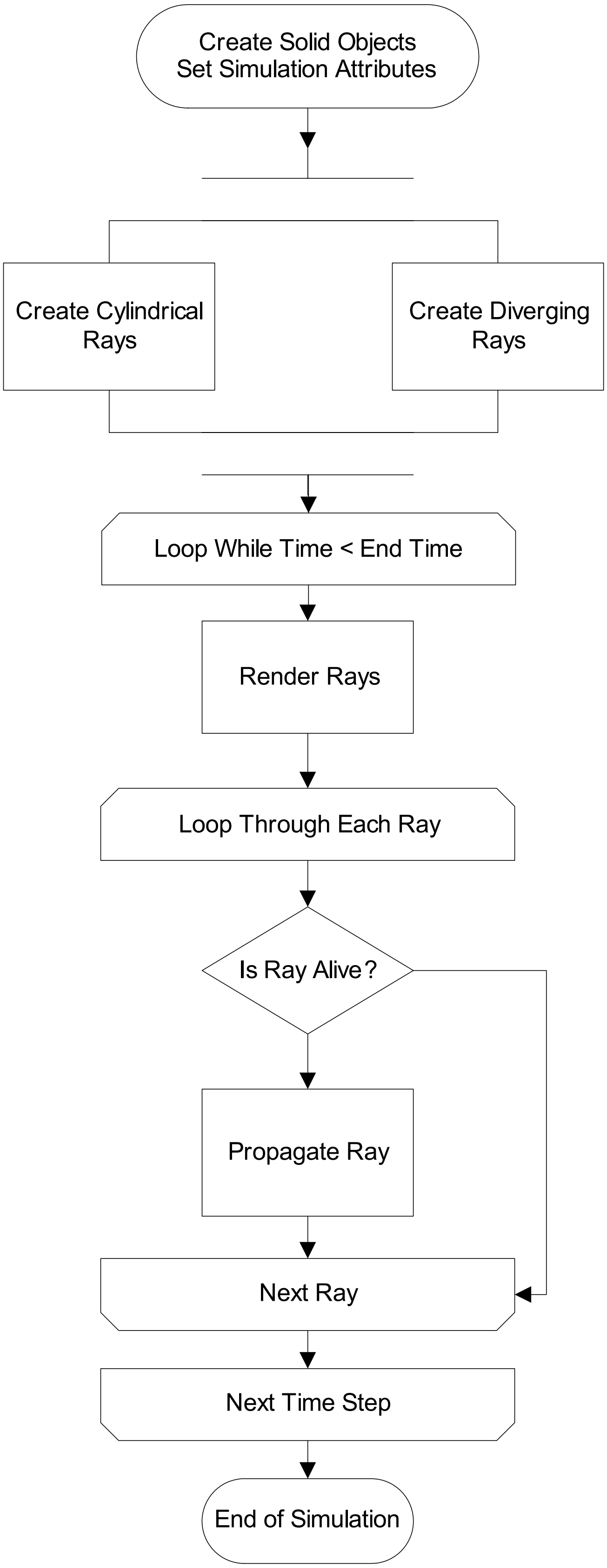

Figure 3.7: Simulation Flow Chart

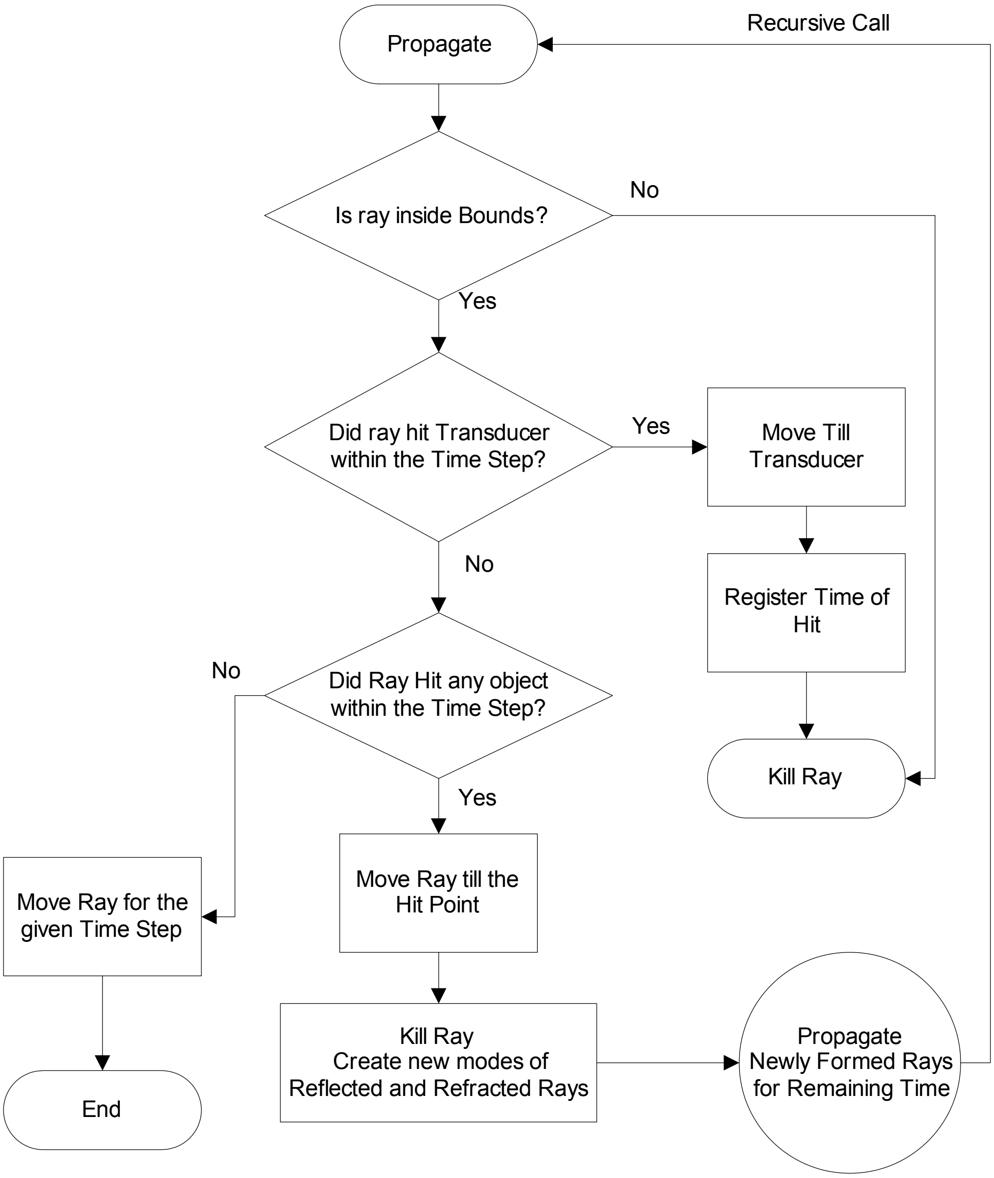

Figure 3.8: Ray Tracing Algorithm

CHAPTER 4

GEOMETRY MODELING

4.1 CONSTRUCTIVE SOLID MODELING

A CAD user interface is used to model the geometry for ultrasonic simulations. When combined with some computer graphics output, the CAD solid model has many uses in modeling. First, the user can visualize the geometry. He or she can position the transducer relative to the part in 3-D space. Secondly, intersections of vectors and the geometry can be calculated. The beam model needs normal vectors, tangents and principal curvatures. It also needs to know if a given point lies on the exterior, surface or interior of the object. The point test is used to keep track of field locations relative to the probe, part and flaw.

The solid model can be done either by using cylindrical or cubical geometry or by importing quad surface meshes. The basic geometry of cylinders and cuboids can be added in Boolean operations to make complex geometries. Figure 4.1 shows a complex geometry made from only cylinders. The cylinder axes can be oriented in any direction to create complex structures.

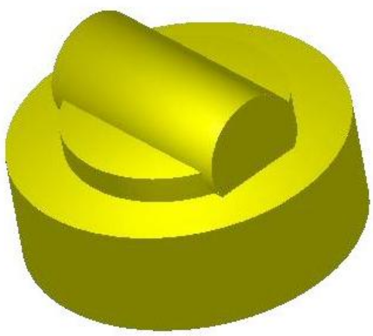

Figure 4.1: Complex Geometry made of Cylinders

Figure 4.2 shows another example of a complex part made from a cylinder and two cuboids. The cuboids also can be oriented in any direction and can be positioned anywhere on the part.

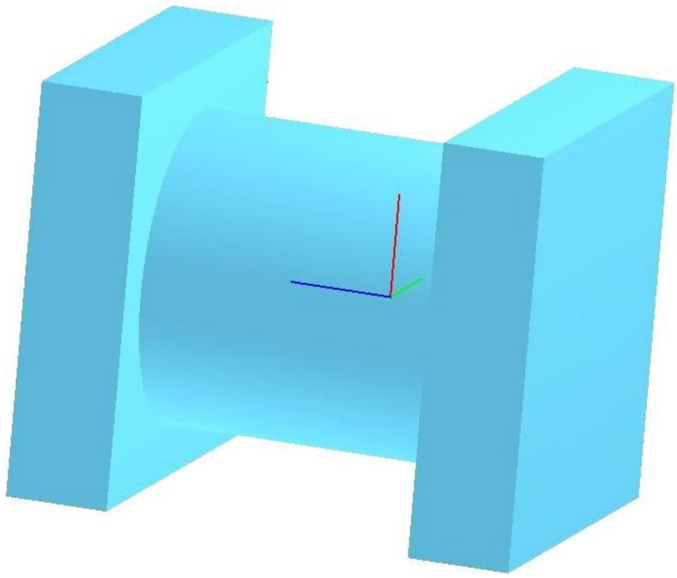

Figure 4.2: Complex Geometry made of Cylinders and Cuboids

Similarly, pipe geometry can be modeled as two coaxial cylinders each corresponding to the inner and outer radii.

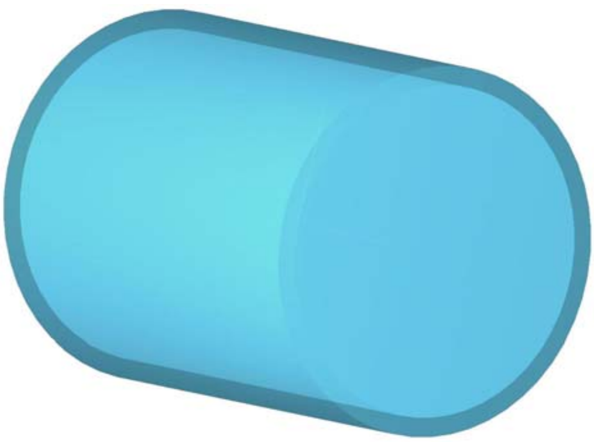

Figure 4.3: Pipe Geometry

4.2 IMPORTED GEOMETRY

Very complex geometries cannot be modeled by just using cylinders and cuboids. In such cases, the geometry can be modeled easily in any CAD software and can be imported into the simulation software. The geometry must be surface meshed using quad elements. Quad elements are elements made of four vertices that lie in the same plane. Figure 4.4 shows a calibration block with flat bottom hole. The geometry was created and meshed in ANSYS and was imported.

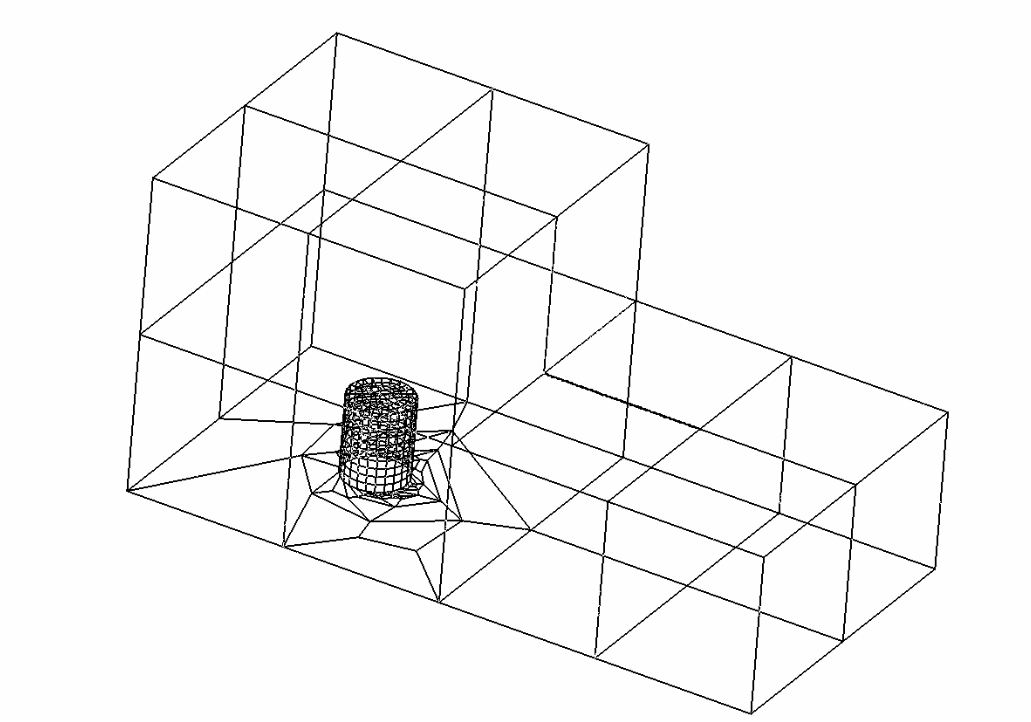

Figure 4.4: Imported Flat Bottom Holed Calibration Block

4.3 CYLINDRICAL INTERFACE CALCULATIONS

The first step in a ray based ultrasonic simulation is to find the intersection point of any ray with the geometry. In case of a cylindrical geometry, the intersection point is found analytically by using geometrical rotations and transformations. The ray is first projected on to a plane perpendicular to the axis of the cylinder. Then the intersection point of the ray with the projected circle of the cylinder is found. This intersection point is used to find the actual intersection point on the surface of the cylinder. The procedure used is described in more detail below.

The global coordinate system is transformed into a local coordinate system with the cylinder axis as the Z-axis. This is done by using matrix transformations. The transformation matrix T is given by Equation(4.1). Here ***n*** is the vector corresponding to the axis of the cylinder; $\boldsymbol{p_1}$ and $\boldsymbol{p_2}$ are vectors mutually perpendicular to each other and to ***n*** and (c_x, c_y ,c_z) is the coordinate corresponding to the center of the base of the cylinder. The vectors are shown in Figure 4.5.

$$T = \begin{bmatrix} n_i & n_j & n_k & c_x \\ p_{1i} & p_{1j} & p_{1k} & c_y \\ p_{2i} & p_{2j} & p_{2k} & c_z \\ 0 & 0 & 0 & 1 \end{bmatrix} \tag{4.1}$$

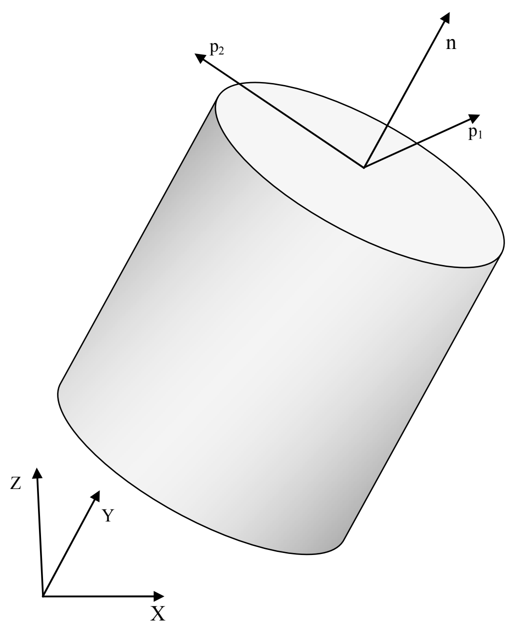

Figure 4.5: Cylinder Intersection

After transforming to the local coordinate system, the ray and the cylinder are projected to the local XY plane. This is done by simply setting the Z coordinates zero. The cylinder is now represented by a circle on the 2-D plane. Now the intersection point of the ray with the circle is found out. Two cases arise; the line either intersects the circle in 2 points or does not intersect at all. The case where the line is tangential to the circle is ignored, as it is a limiting case.

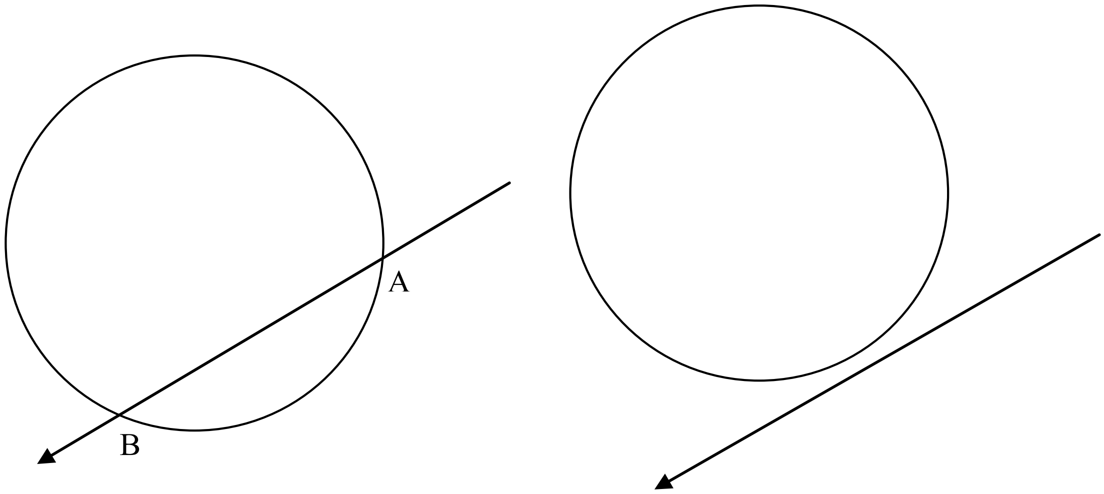

Figure 4.6: Two Possible Cases of Cylinder Intersection

Figure 4.6 shows the two possible cases that can arise. In case 2, there is no intersection of the ray with cylinder. In case 1, the ray intersects the cylinder at two points A and B. The actual point of intersection is chosen from these two points based on the position of the ray. The normal to the surface at the point of contact is also calculated. After the intersection point is found, it is transformed back to the global coordinate system. The inverse transformation matrix is used for this operation.

4.4 QUAD ELEMENT INTERFACE CALCULATIONS

A Quad element is defined by its four vertices and a normal to the plane of the vertices. The intersection point of a ray with a Quad element is comparatively easier to find than the intersection with a cylinder. It is usually done as a two-step process.

First, the intersection of the ray with the plane containing the vertices is found. We can always find the intersection point of the ray with the plane unless the ray is parallel to the plane. Equations(4.2) give the steps involved in find the intersection point.

$$
\begin{aligned}
d &= -(A_x \times n_i \;+\; A_y \times n_j \;+\; A_z \times n_k) \\
t &= \frac{x \times n_i \;+\; y \times n_j \;+\; z \times n_k + d}{(\bar{n} \times \bar{r})} \\
P \;&=\; (x \;+\; t \times i,\; y \;+\; t \times j,\; z \;+\; t \times k\,\_)
\end{aligned}
\tag{4.2}
$$

Two cases arise after the intersection point P is found which are shown in Figure 4.7. In the first case, the intersection point P lies inside the Quad element whereas in the other case, it lies outside the element.

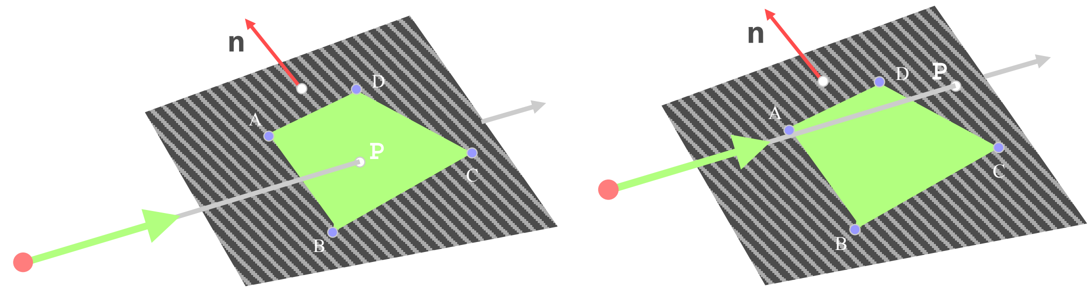

Figure 4.7: Two Cases of Quad Intersection

A simple numerical test is used to distinguish between the two cases as shown in Equation(4.3). If the point lies inside the quad, the sum of the angles subtended by the sides of the quad at P is 2π. In the other case, the sum of the angles is not equal to 2π.

$$\angle APB + \angle BPC + \angle CPD + \angle DPA = 2\pi \qquad (4.3)$$

For calculation purposes, to account for numerical floating-point errors, the sum of the angles is taken to be approximately equal to 2π. In Equation(4.4), the value of Δ is taken to be a very small positive number to take care of numerical errors both in the value of π as well as in the calculations.

$$2\pi - \Delta \leq \angle APB + \angle BPC + \angle CPD + \angle DPA \leq 2\pi + \Delta \qquad (4.4)$$

4.5 CUBOID INTERFACE CALCULATIONS

A cuboid element is made of six Quad elements; Top, Bottom, Left, Right, Front and Back. For finding the intersection with a cuboid, the intersection point of the ray with each of the six quads is found. Then the point that is closest to the head point of the ray along the ray direction is chosen as the intersection point.

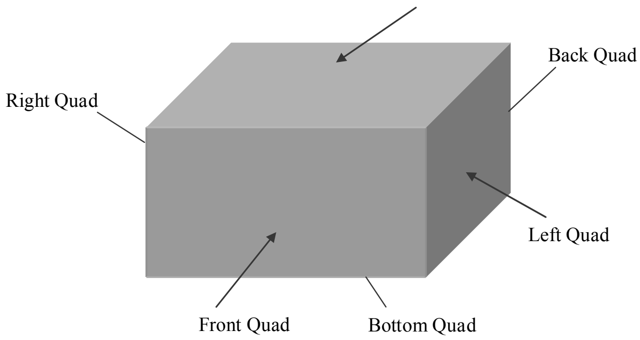

Figure 4.8: Cuboid Definition

CHAPTER 5

SIMULATION STUDIES

5.1 CALIBRATION BLOCK

Simulation studies were done in a calibration block to validate the ray tracing model and the field model. The calibration block is a 1-inch thick aluminum block. The dimensions used in the simulations are given in Figure 5.1.

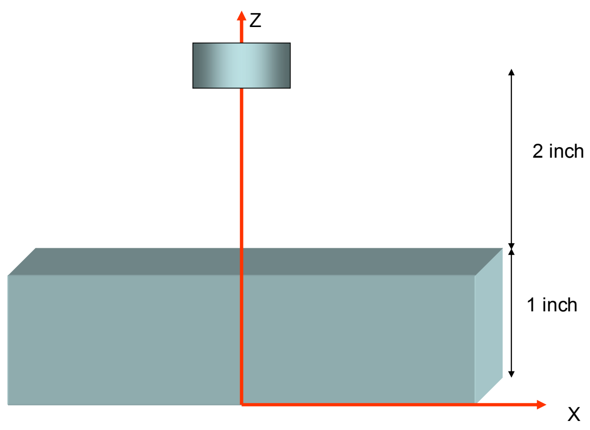

Figure 5.1: Calibration Block Geometry

The simulations on the calibration block were done to verify the arrival time of the ultrasonic waves. Studies were also done to show the independence of the received A-Scan with the number of rays. The discretization of the beam into different numbers of rays has no effect on the received signal as long as there is no curvature on the part. This is shown in Figure 5.2 and Figure 5.3.

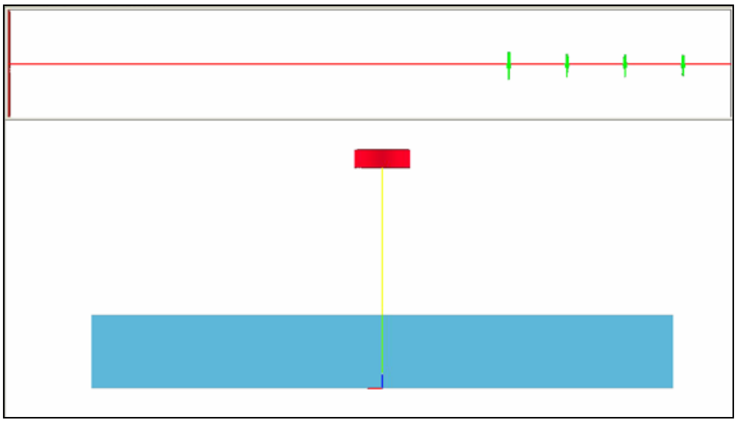

Figure 5.2: Simulation on a Flat Block with 1 ray

In the first case the simulation is done with a single ray and with 40x40 (1600) rays in the second case. There is no difference in the received signal amplitude as the initial energy is distributed to all the rays and hence the sum of the received signal is constant in all the cases. Moreover, from Figure 5.4 it is clear that the normalized received intensity does not depend on the number of rays for a flat geometry.

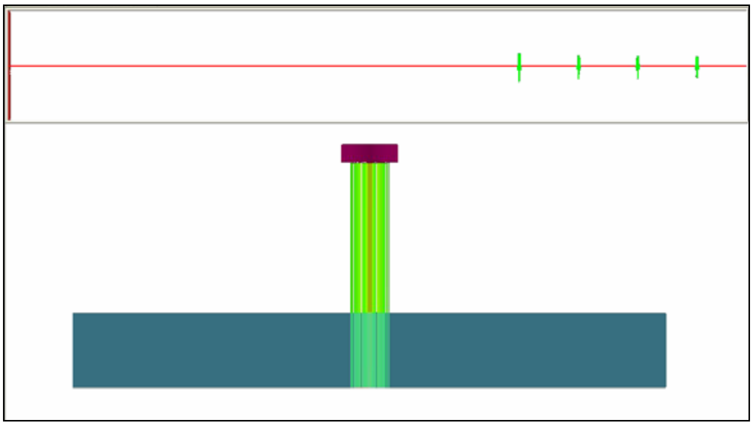

Figure 5.3: Simulation on a Flat Block with 40x40 rays

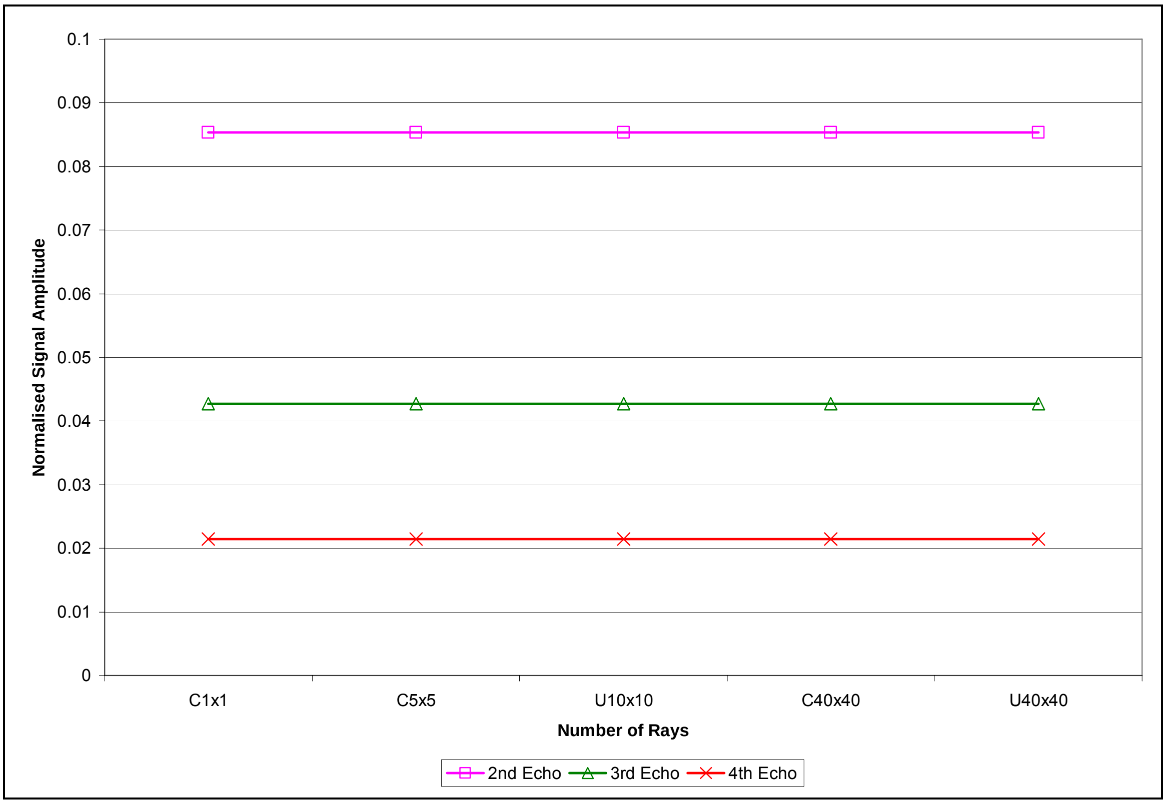

Figure 5.4: Convergence Study on a Flat Plate

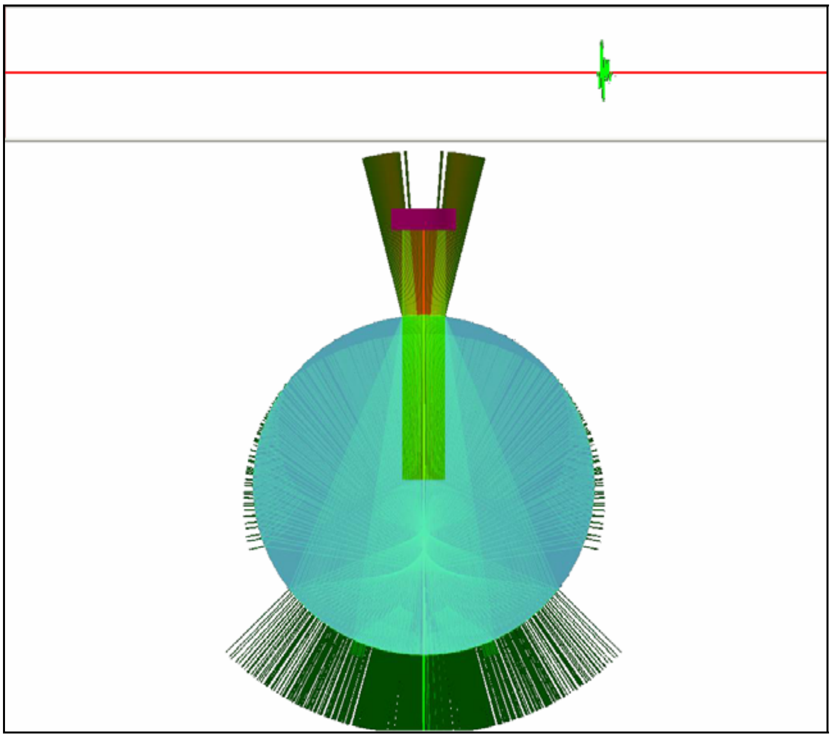

Figure 5.5: Inspection of a Curved Surface

However, the discretization of the beam into rays does play a role if there is a curvature in the geometry. For example, in Figure 5.5, a cylindrical surface is inspected. As expected, the amplitude of the received signal varies with the number of rays used. From Figure 5.6, it can be concluded that the received signal amplitude remains constant after for more than 20x20 rays. Hence, it is sufficient to use 20x20 numbers of rays for the inspection of the given curved surface.

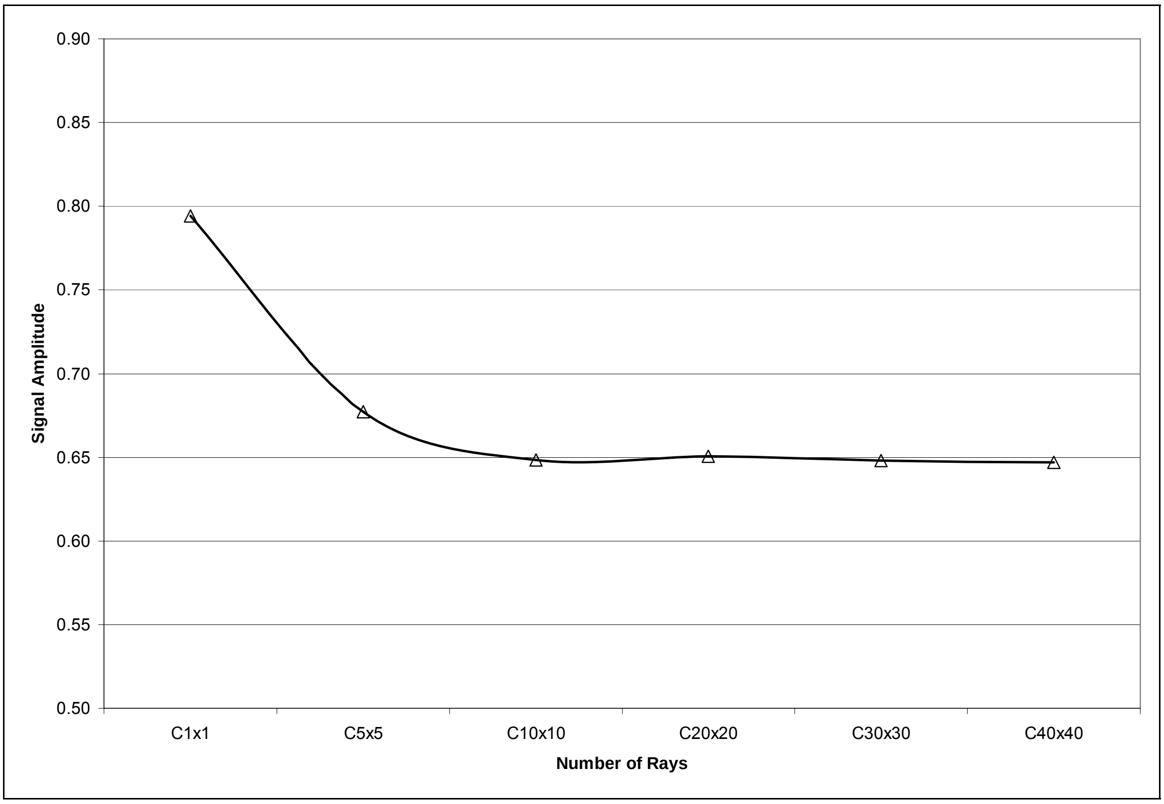

Figure 5.6: Convergence Study on a Curved Surface

5.2 SIMULATIONS IN A BLOCK WITH FLAT BOTTOM HOLE

A standard calibration block with a flat bottom hole is also used to validate the model. The calibration block is 200mm long with a step. The flat-bottom hole is 20 mm in diameter, 25 mm in height and is centered at 50 mm from the end. The simulation was done using a ½-inch diameter, 5MHz transducer. The beam spread was calculated to be 2º assuming a 6dB drop. Figure 5.7 shows the case when the transducer is directly above the flat-bottom hole.

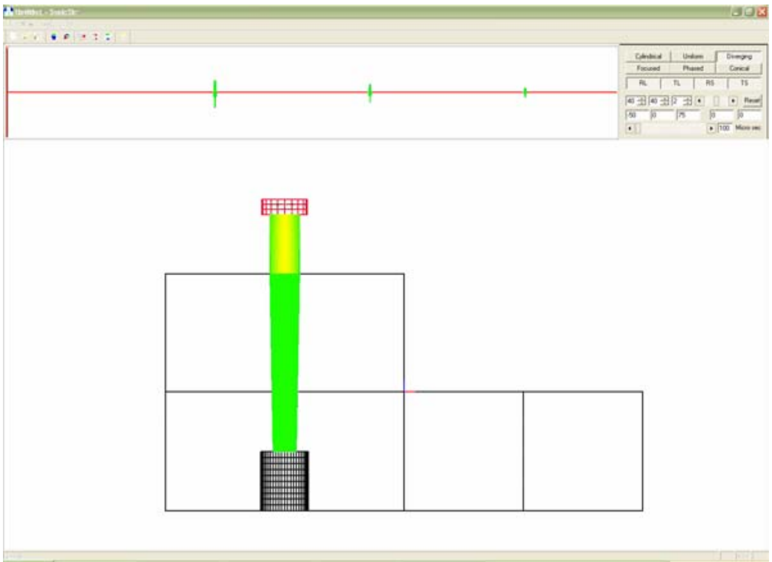

Figure 5.7: Inspection over a Flat Bottom Hole

The transducer was moved at a constant height above the flat-bottom hole to create a B-Scan. Figure 5.8 shows the B-Scan of the flat bottom hole. The figure on the left is the complete B-Scan, while the figure on the right is the response of the back wall and flat bottom hole.

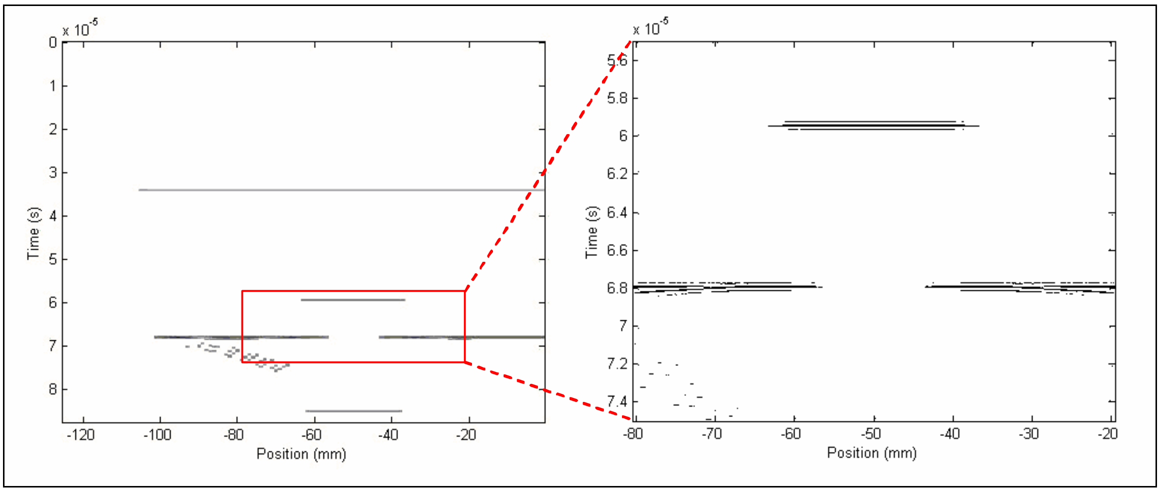

Figure 5.8: B-Scan of the Flat Bottom Hole

Figure 5.9 shows the response from the back-wall as well as the flat bottom hole. It can be seen that the response from the flat bottom hole tapers at the edges of the hole and there is a signal both from the FBH as well as from the back wall at the edges of the hole.

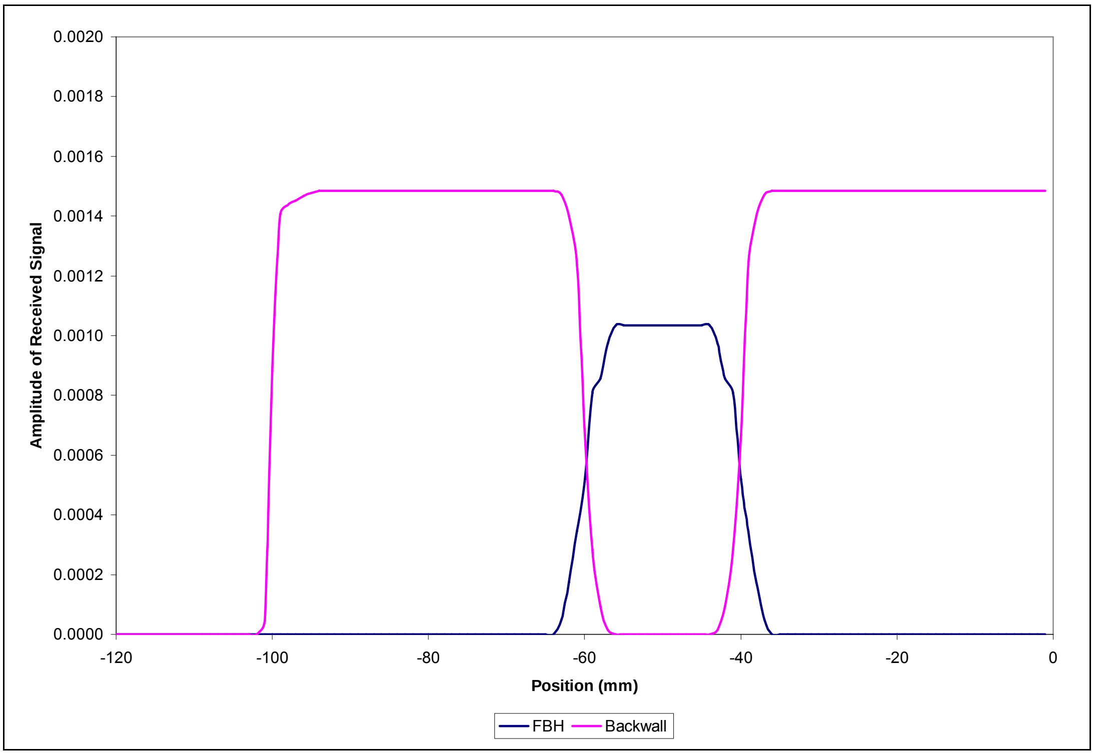

Figure 5.9: Response from FBH and Back Wall

5.3 PIPE SIMULATIONS

Ultrasonic simulations were done on a large pipe with EDM notches. As discussed in the geometry-modeling chapter, the pipe is modeled as two coaxial cylinders with different radii. The material of the pipe is steel and the surrounding medium is modeled as water as it is an immersion testing. The EDM notches are modeled as surface opening cuboids of appropriate dimensions.

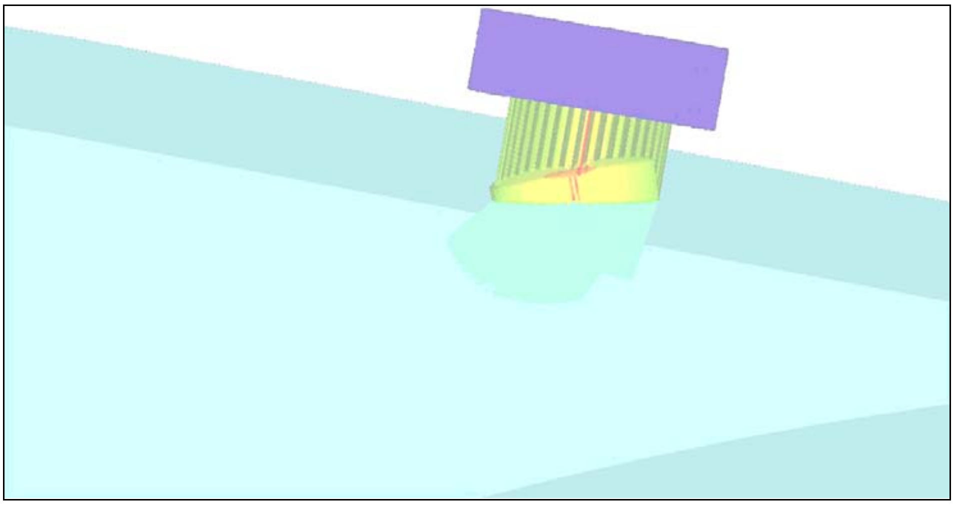

Figure 5.10: Pipe with an Ultrasonic Beam Simulation

The ultrasonic beam is modeled as a collection of beams as shown in 3D in Figure 5.10. The incident beam produces both shear and longitudinal waves inside the pipe specimen. In Figure 5.11, the transducer is so angled so that the incident beam is above the first critical angle. Hence, only shear rays are produced inside the pipe circumference.

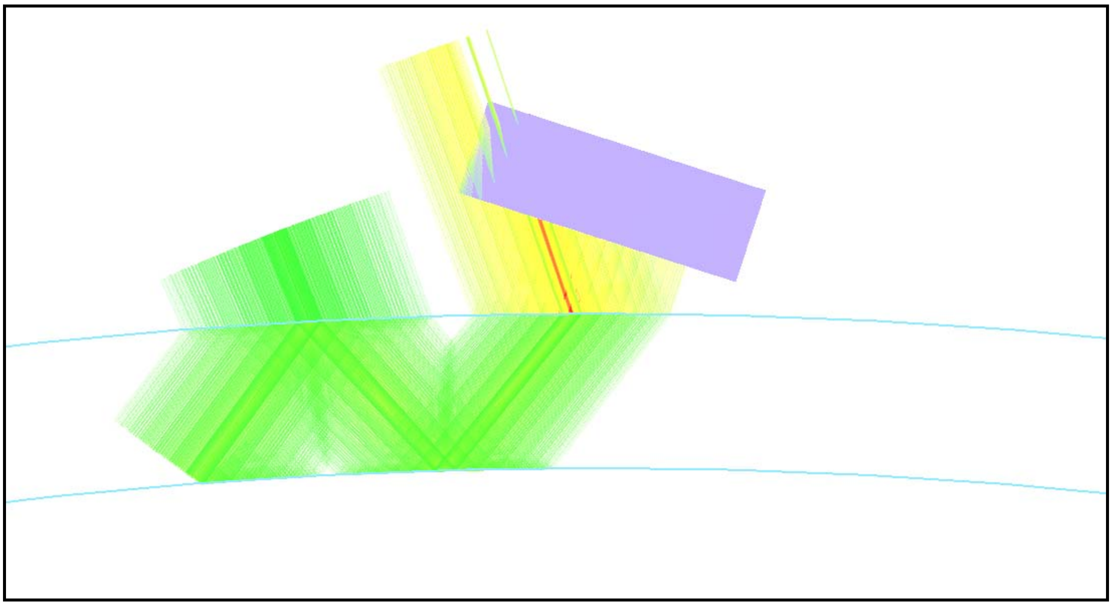

Figure 5.11: Pipe Simulations with no Defect

The EDM notch of appropriate dimension is modeled in Figure 5.12. The figure shows all the rays that come back to the receiver after reflection from the crack.

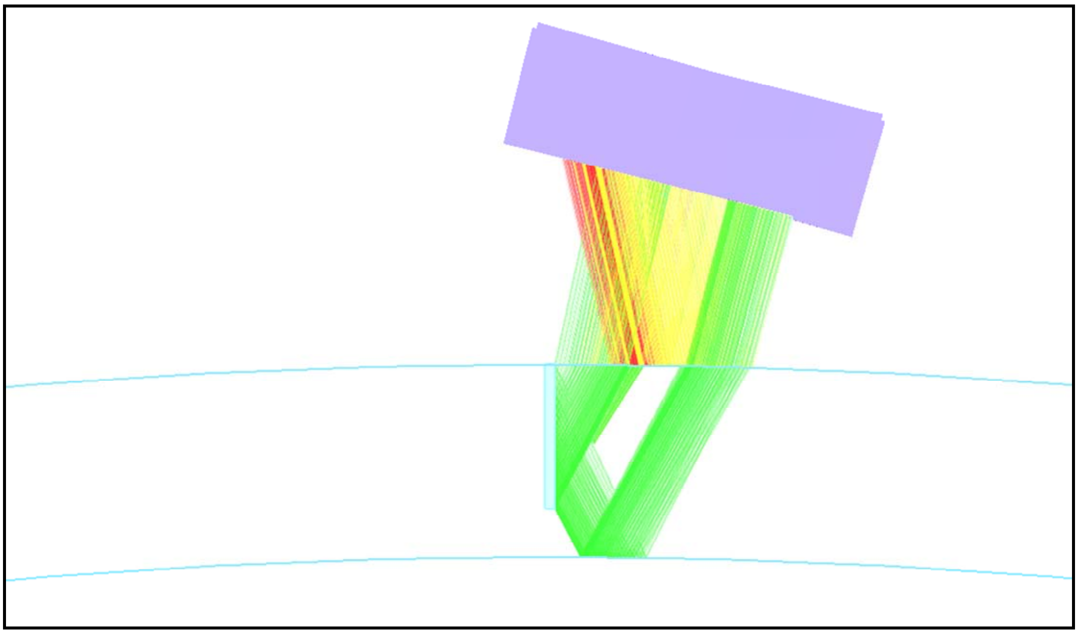

Figure 5.12: Simulation with EDM Notch

The simulations were carried out at different angles of the transducer with the vertical. The defect indications were clearly visible at particular angles only. Hence, the simulation can be used to choose the particular angle at which the transducer is most sensitive to defects of different sizes.

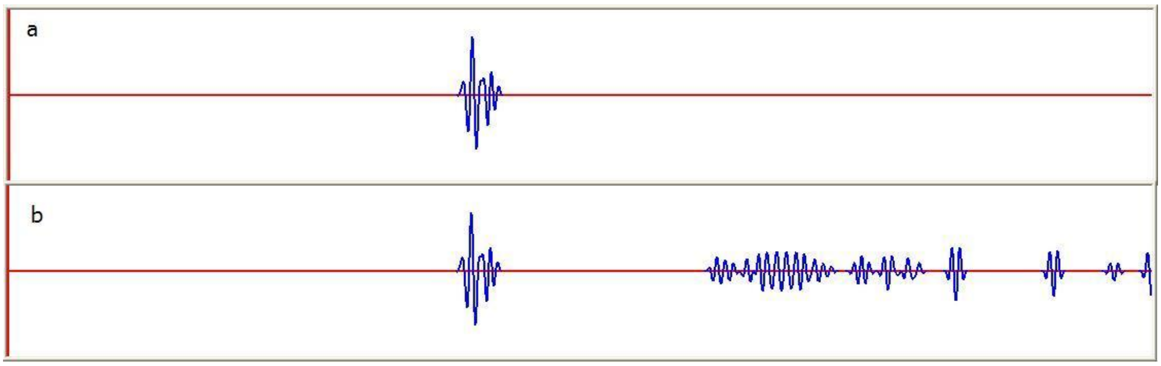

Figure 5.13: A-Scan at 6º Transducer angle (a) without notch, (b) with Notch

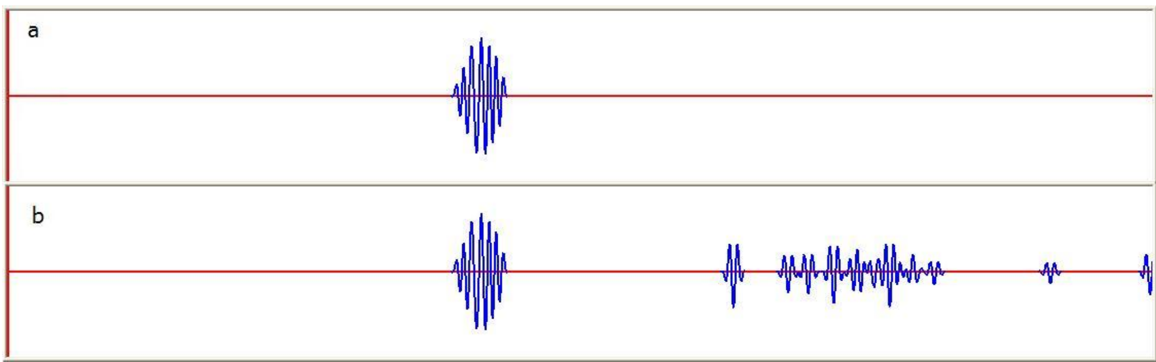

Figure 5.14: A-Scan at 8º Transducer angle (a) without notch, (b) with Notch

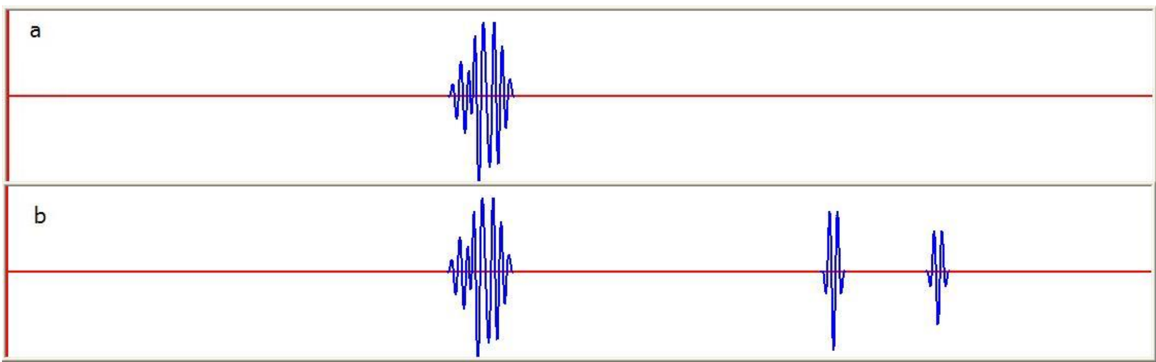

Figure 5.15: A-Scan at 10º Transducer angle (a) without notch, (b) with Notch

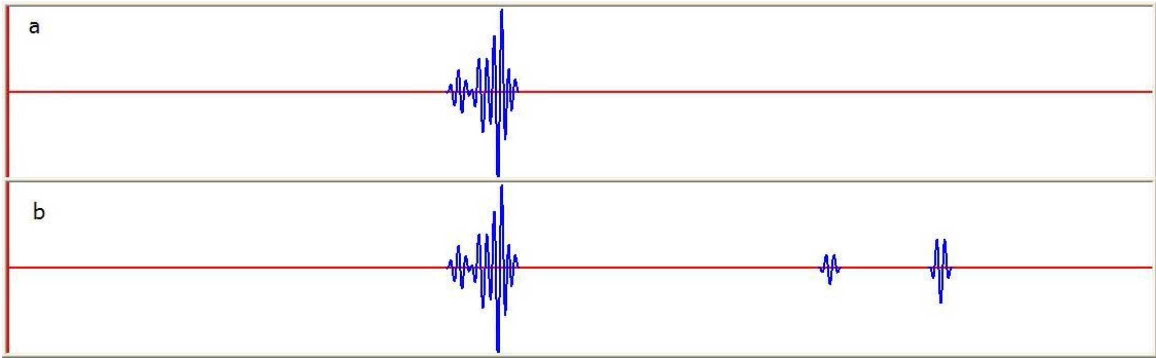

Figure 5.16: A-Scan at 12º Transducer angle (a) without notch, (b) with Notch

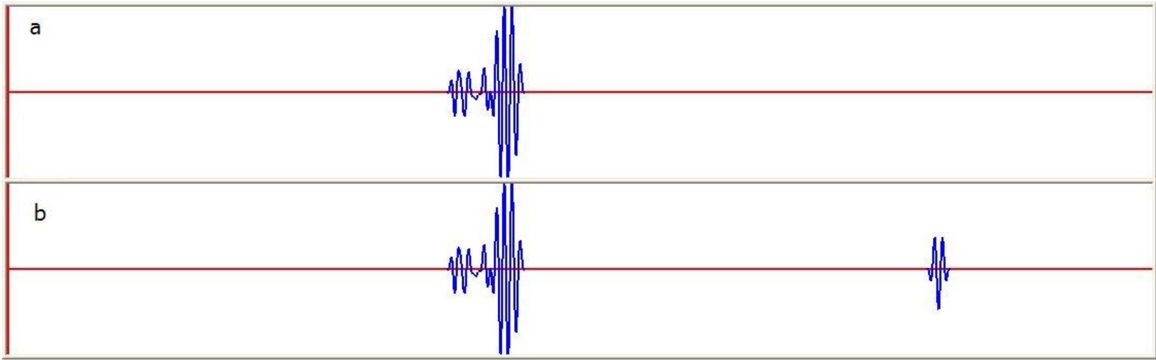

Figure 5.17: A-Scan at 14º Transducer angle (a) without notch, (b) with Notch

From the analysis of A-Scans from Figure 5.13 to Figure 5.17, it can be concluded that an angle of 12° or more is suited for detection of notches and other defects in the pipe. Moreover, the first critical angle of the specimen is 13°. Hence, in Figure 5.17, there is only one flaw indication, whereas in Figure 5.16, there are two indications, one each from the shear waves and longitudinal waves propagating inside the pipe. Thus, the optimum angle of transducer can be obtained and can be subsequently used to choose experimental parameters.

5.4 SIMULATION OF CREEP WAVES IN PIPES

Creep waves are waves that are generated in thin pipes and travel along the circumference of the pipe. It is also possible to simulate creep waves by adjusting the angle so that the beam is incident on the pipe at the critical angle. As the angle of incidence plays an important role in the generation of creeping wave in the incident material, the ultrasonic transducer is inclined to the accurate angle so that the incident waves will induce creeping waves into the material. Figure 5.18 shows the simulation of creep waves along the pipe circumference. The emitting transducer is shown as blue and the receiving transducer is represented in red. The waves propagate through the whole of the circumference to reach the receiver.

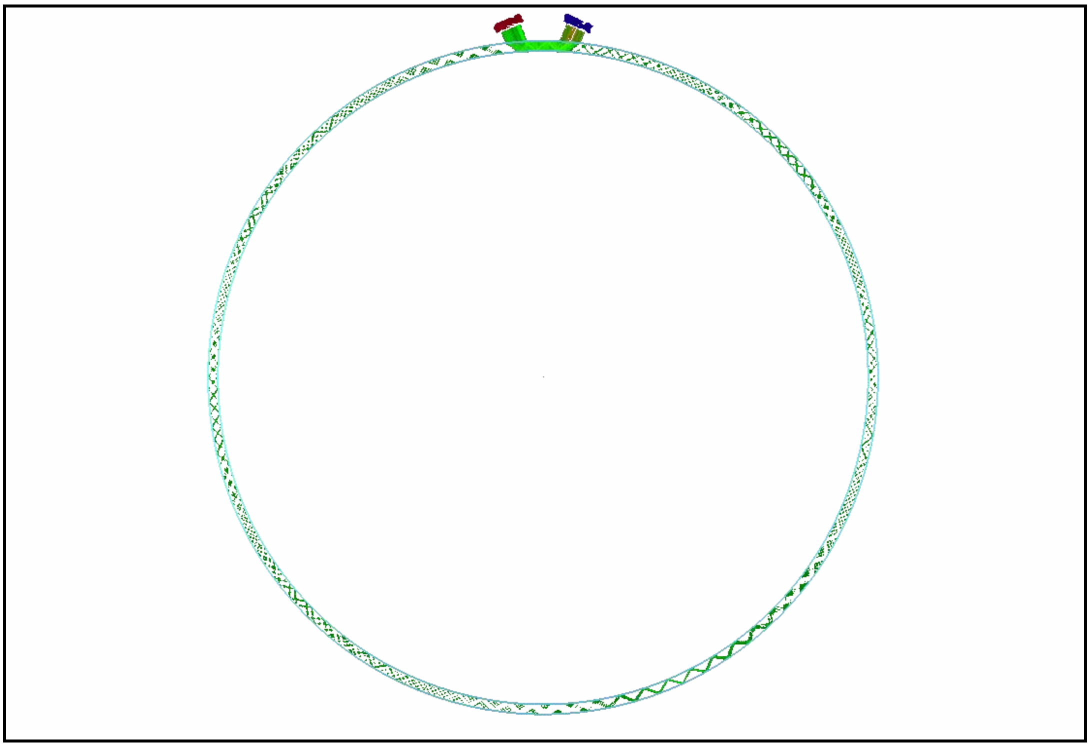

Figure 5.18: Simulation of creep waves

Figure 5.19(b) shows the effect of a 9mm high notch in the test specimen in the top. With the notch, the amplitude of the first signal is reduced. In addition, there are some more signal indications present in the A-Scan of the specimen with notch. These simulations can be used to predict the signal that would be obtained with different experimental parameters.

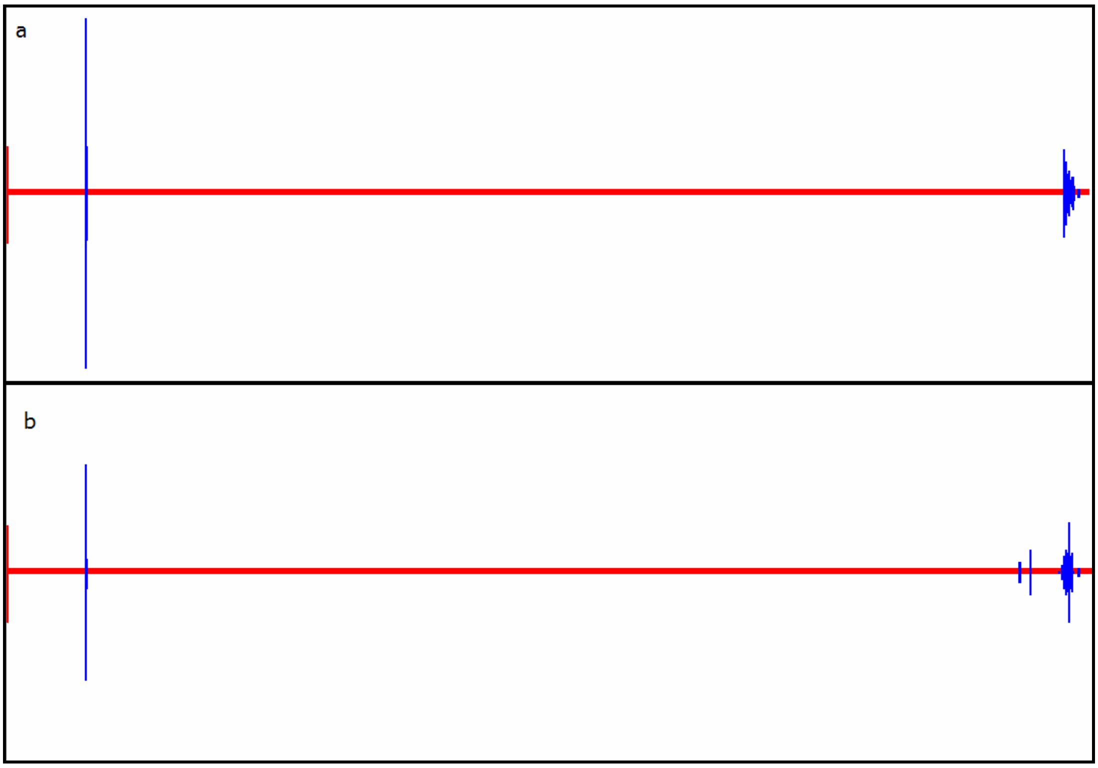

Figure 5.19: A-Scan of a pipe (a) without notch and (b) with a 9mm Notch

CHAPTER 6

INSPECTION OF THIN PIPES

6.1 PROBLEM DESCRIPTION

The ultrasonic simulation program was used to design an inspection method for testing the weld plug in a thin nuclear fuel rod. The fuel rod is a thin walled cylinder with a wall thickness of 0.4 mm. The entire fuel pin is only 6.5 mm is diameter. Figure 6.1 shows the fuel pin assembly with and without the end plug. The welding of the end plug is very critical as the whole integrity of the fuel rod depends on this weld.

Figure 6.1: Fuel Pin Assembly

Inspection of such thin walled cylinders poses several difficulties if done conventionally. First, the dimensions of the cylinder are so small that the most of the transducers are very big for inspection. Hence, a focused transducer is chosen to reduce the beam footprint on the front wall of the cylinder. Moreover, the weld is accessible from only one direction. Hence, an angle-beam inspection technique has to be used.

For inspection of thin walled specimens, it is better to choose a high frequency of inspection to increase resolution. Hence, the frequency of inspection is chosen as 15 MHz. The small size of the specimen also rules out any contact inspection testing. Therefore, a water-immersed inspection was chosen to be the ideal option.

6.2 Initial Optimization Studies

Initial studies were done to assess the feasibility of the inspection of the end plug weld by using ray tracing. These studies were done to find the optimum position of the transducer that is ideal for testing. A commercially available 15 MHz, ¼-inch diameter transducer with a focusing distance of 1½ inch is chosen for inspection.

The studies were done to find the standoff distance as well as the angle of inspection. The distance of the center of the probe from the wall is fixed as 1½ inch to utilize the focus of the transducer effectively. The angle, θ of the probe is also varied from 16º to 23º.

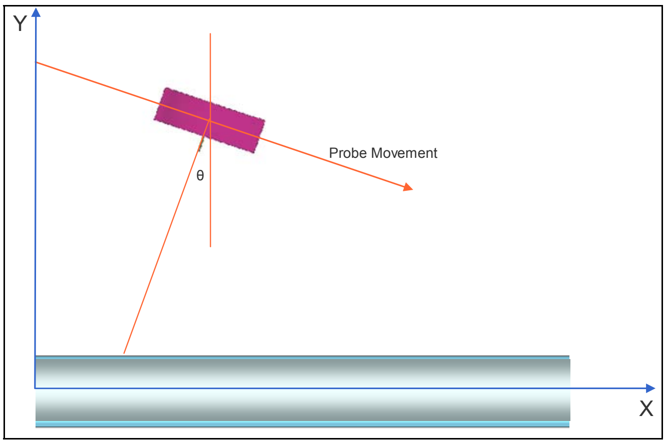

Figure 6.2: Simulation Configuration

The sum of the maximum peak-to-peak values of the received signal is taken as an indication of the effectiveness of the scan position. Figure 6.3 shows the variation of the received energy with respect to transducer position as well as the transducer angle.

From Figure 6.3, it can be seen that a transducer angle of 18º to 19º gives the maximum response from the front wall. In addition, it can be seen that the transducer position is critical in getting a proper response. Even a variation of 1mm causes a drastic change in the received signal.

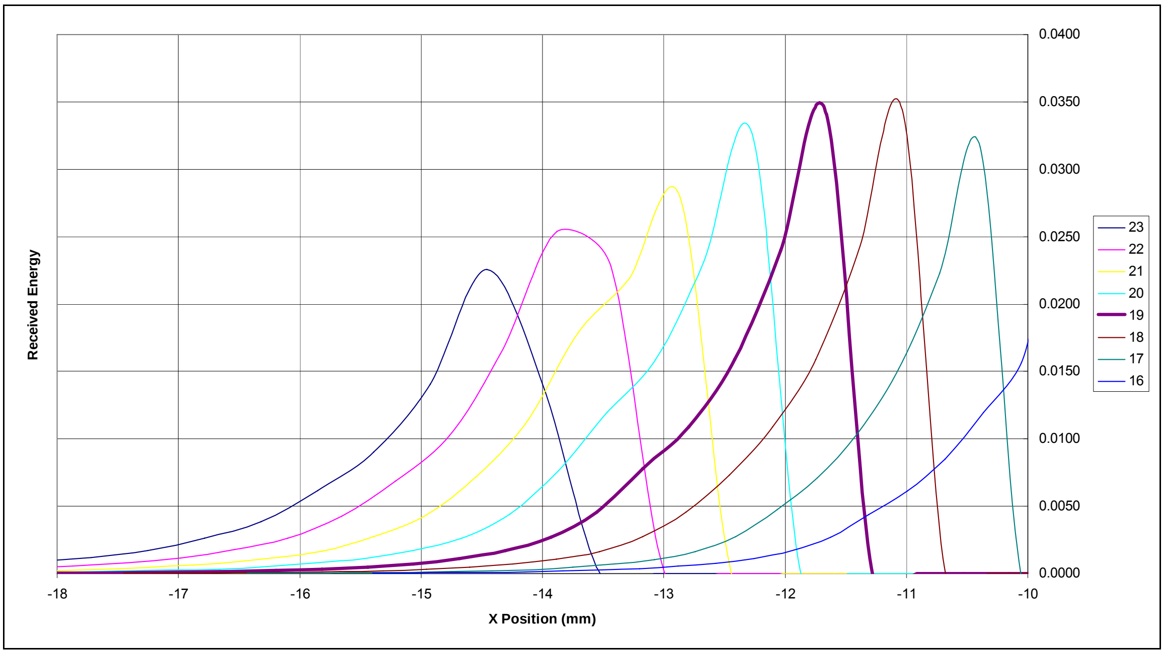

Figure 6.3: Variation with Probe Position

From the results obtained by simulations, it was decided to use 19º as the angle of inspection. Moreover, the standoff distance was chosen to be 12 mm horizontally with a corresponding standoff distance of 35 mm vertically.

6.3 EXPERIMENTAL SETUP

Based on the initial optimization studies, an experimental setup was built to validate the results experimentally.

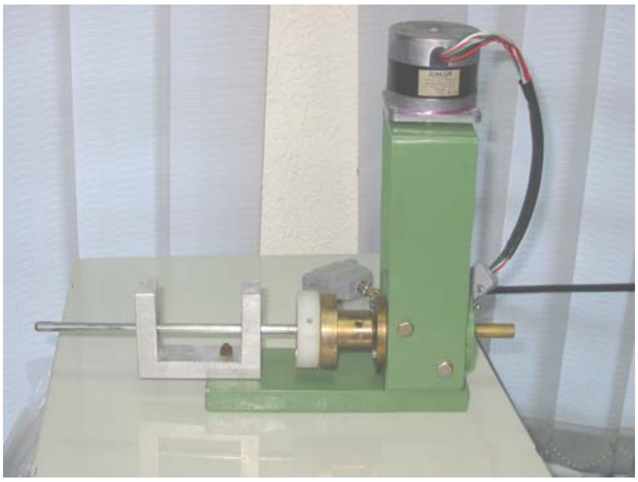

Figure 6.4: Tube Holder with a Stepper Motor

Figure 6.4 shows the tube holder with supports. The tube is mounted on two bushes that prevent the wobble in the tube as it is rotated. The tube holder has the facility to rotate the tube about its axis. This is required to inspect the entire weld or the front wall of the cylinder. The stepper motor can be connected to a controller and then to the computer. A Lab-VIEW program is used to control the position of the tube.

Figure 6.5: Experimental Setup

The transducer is mounted on a XY-Scanner as shown in Figure 6.5. The transducer can be moved along the XY Plane with the help of the two stepper motors, a positional controller and interfacing software.

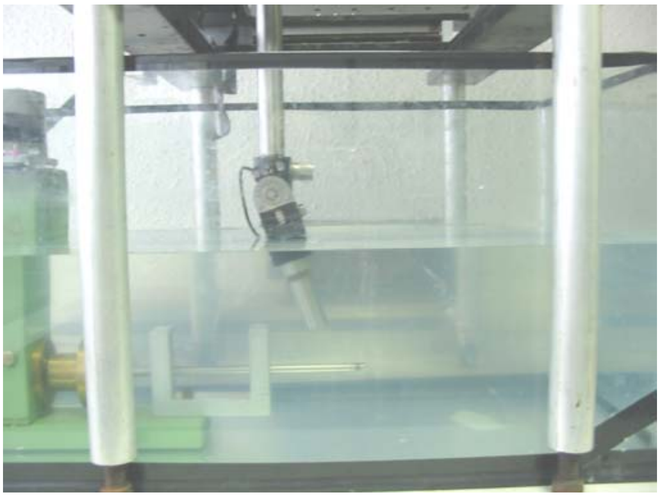

Figure 6.6: Immersion Setup showing the Probe Holder

In addition, the probe holder shown in Figure 6.6 has the ability to be tilted to any angle. The indication of the tilt angle can be read from an angular scale mounted on the holder. With the help of this holder, the transducer can be positioned to the requisite 19º angle for inspection. The 2-Axis XY degree of freedom along with the rotational axis of the tube makes it possible to position the transducer to inspect any section of the tube wall.

The transducer was powered by a Panametrics PR500 Pulser-Receiver. The signal was sampled at a sampling rate of 100 MHz, which is sufficient for a 15 MHz transducer.

6.4 Results and Discussion

To validate the results of the simulations, a line scan was performed by moving the transducer at a constant height along the axis of the tube. The scan path and the details of the scan are shown in Figure 6.7.

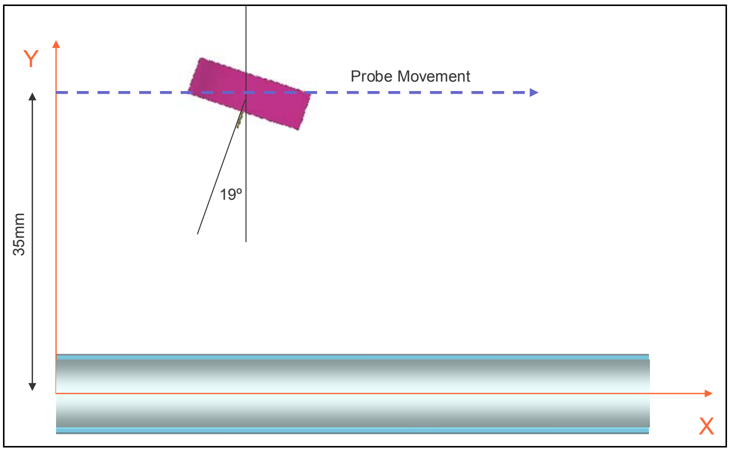

Figure 6.7: Scan Path and Configuration

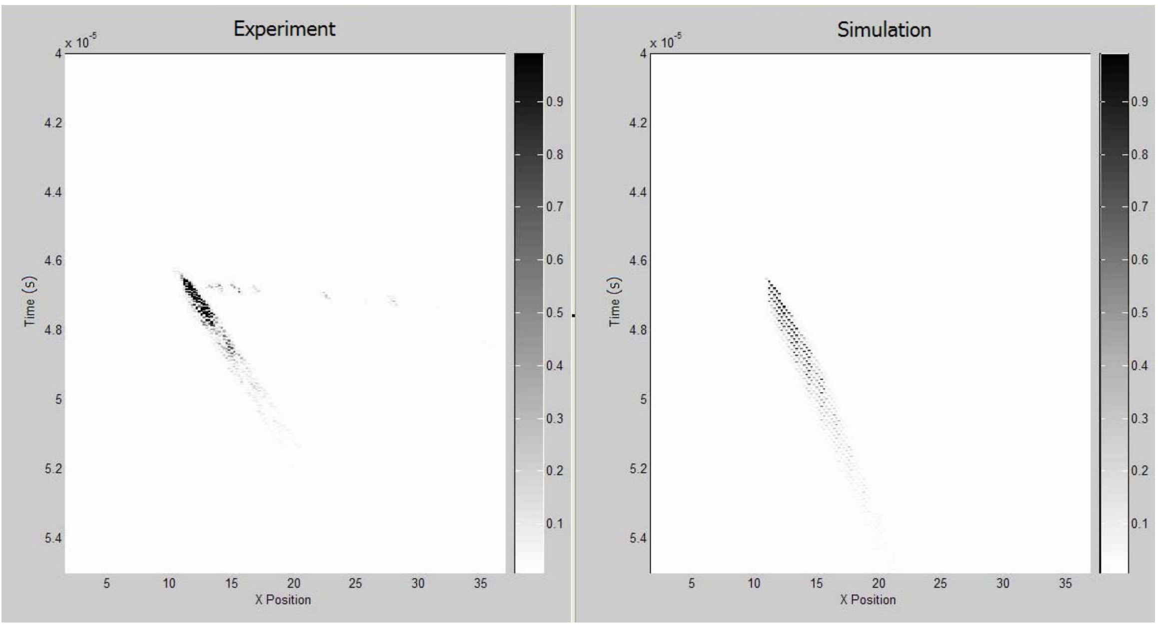

Figure 6.8: B-Scans obtained from Experiment and Simulations

Figure 6.8 shows the B-Scans obtained from the experiment and simulation. The images show good correlation both with the arrival time of the signal as well as the amplitudes of the signals. It can be seen that as the position of the transducer is moved farther from the pipe wall the arrival time increases and the amplitude of the received signal also drops. It is also verified that the signal received is maximum at around 11-13 mm that was predicted during the initial studies.

Figure 6.9 and Figure 6.10 shows the comparison of A-Scans obtained at two different positions of the transducer. It can be seen from the figures that the position and the normalized amplitudes of the first four peaks match reasonably well. However, the match is not that prominent beyond the 5th multiple. This may be due to experimental losses or errors.

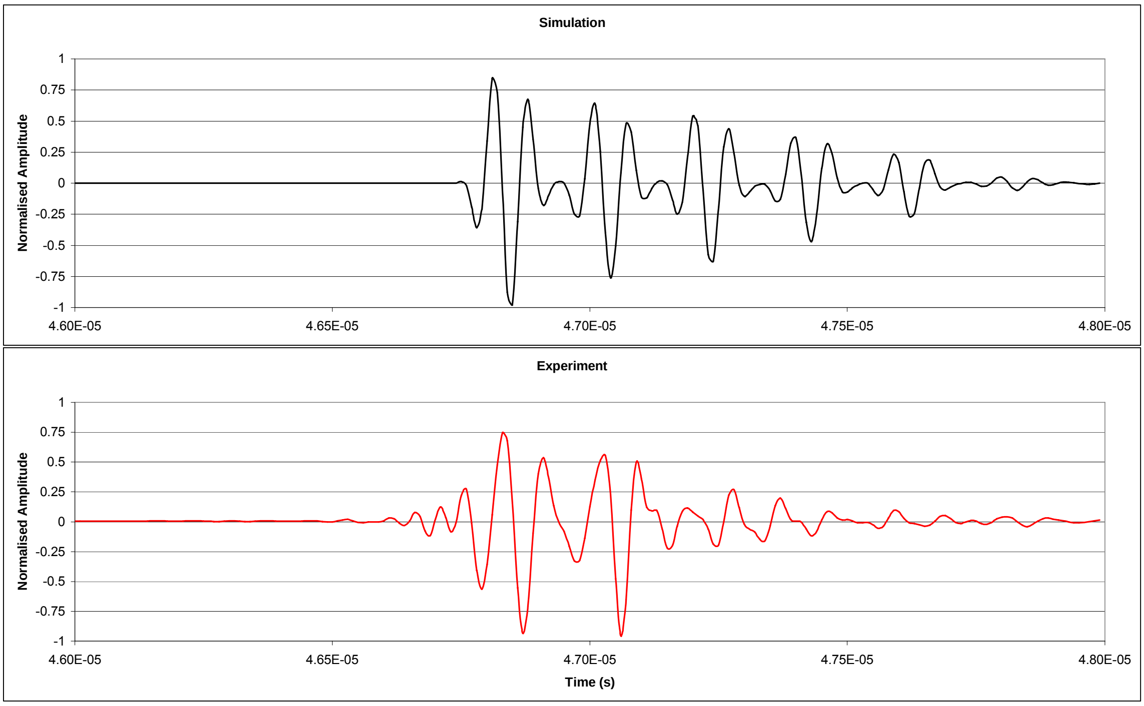

Figure 6.9: Comparison of A-Scan at x=12 mm

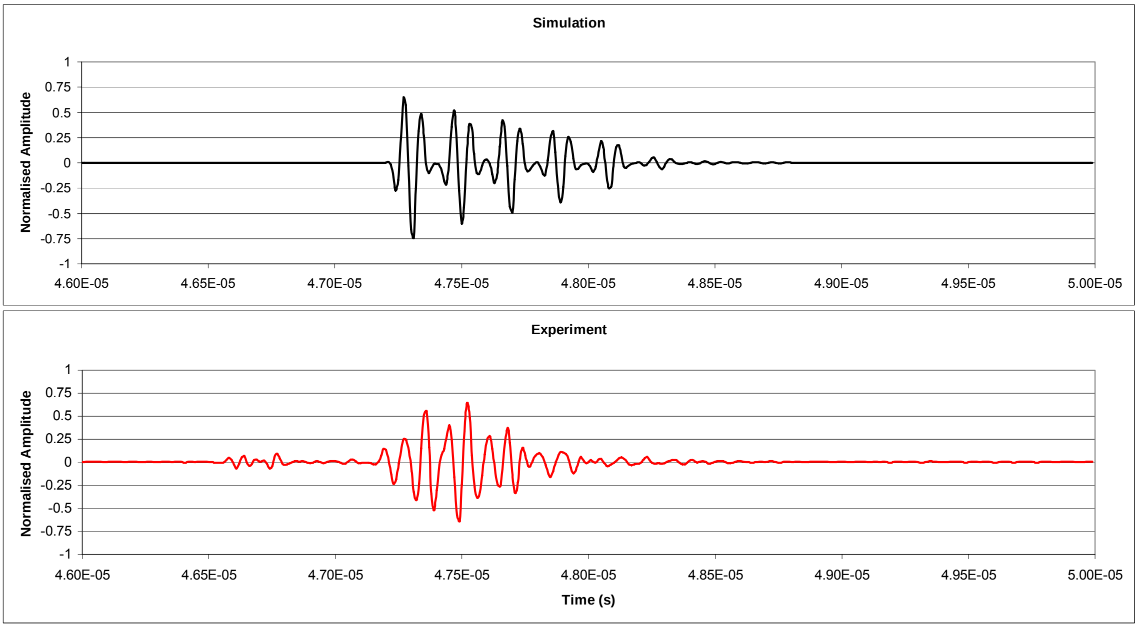

Figure 6.10: Comparison of A-Scan at x=14 mm

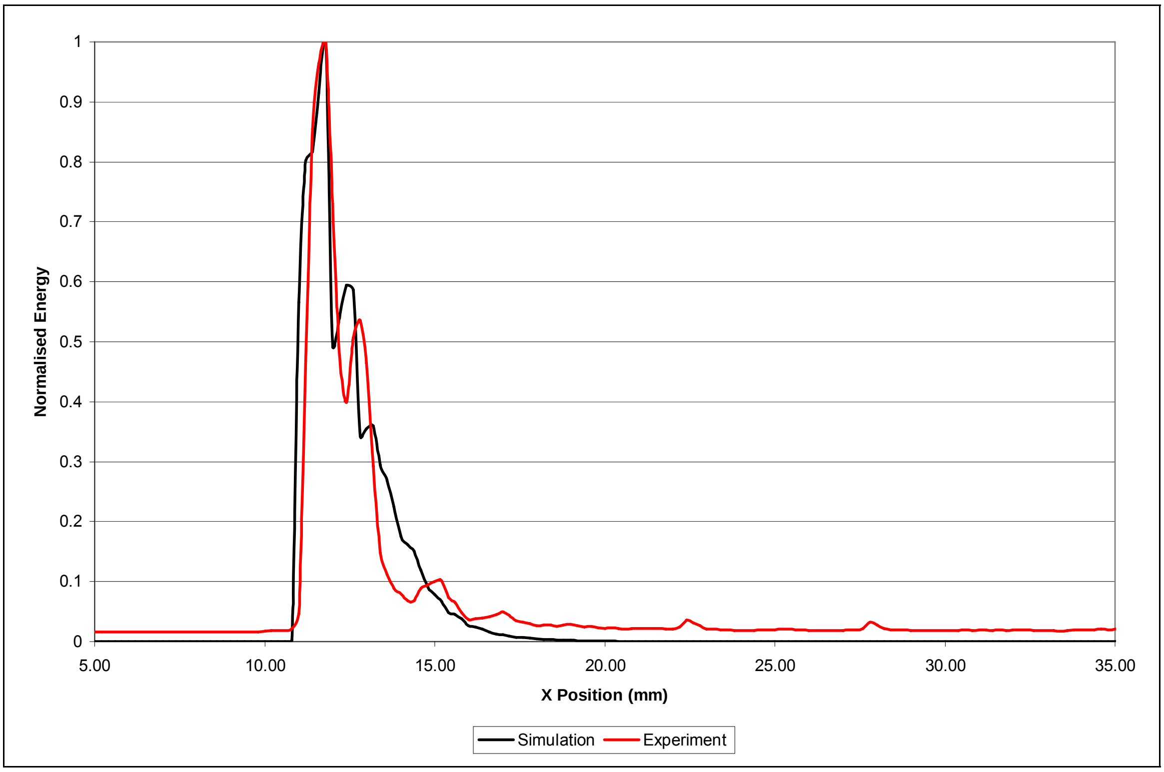

Figure 6.11: Variation of Normalized Received Energy with Probe Position

Figure 6.11 shows the sum of the peak-to-peak amplitudes obtained from simulation as well as experiments as a function of position. Certain key features like the increase in amplitude at around 14 mm are noted both in experiments as well as in simulations.

The results obtained from experiments confirm the validity of the simulations. Further simulation studies in even more complex geometries can be undertaken. Moreover, the simulations can also be used to identify a bad weld region from an actual scan data.

CHAPTER 7

CONCLUSIONS AND FUTURE WORK

7.1 SUMMARY

Ultrasonic simulations using ray tracing offers a practical and quick method to help determine or to optimize ultrasonic probe locations for inspection of complex components. The program provides a ray-trace based assessment initially followed by a displacement or pressure field-based assessment for user-specified probe positions and user-selected components. Immersion and contact modes of inspection are also available. The code written in Visual C++ has an interactive graphical user interface. The program supports geometry modeling as well as transducer modeling.

Simulation studies were done on a flat plate and over a flat bottom hole. The results obtained were represented as either B-Scan or A-Scan. Studies were also done to detect notches in pipes. The resulting A-Scans were used to determine the optimum position of the transducer for pipe inspection.

The program was applied to the inspection of very thin-walled pipes (with 450 μm wall thickness). The weldment (TIG type) of a thin-walled pipe was inspected for poor or lack of welding across the wall thickness over the entire circumference. Ray trace based assessment was done using the program to determine the standoff distance and the angle of oblique incidence for an immersion mode focused transducer. The A-scans and the associated B-Scan images obtained through simulations show good correlation with experimental results, both with the arrival time of the signal as well as with the signal amplitudes.

7.2 FUTURE WORK

- The program can be extended to handle Phased Array probes whose characteristics can be dynamically varied.
- The program can be extended to handle part files directly from CAD software. The program can be used to import common graphic file formats like IGES. This would greatly enhance the usability of the program.
- The model can be extended to include flaw interactions by coupling the ray tracing with numerical flaw models.
- The field calculations of the flat bottom hole can be compared with experimental results from standard calibration blocks.

REFERENCES

1. **Schmerr L.W.** *Fundamentals of ultrasonic non-destructive evaluation: A Modeling Approach*, 1998.

2. **Krautkrämer A. J.** and **Krautkrämer H.** *Ultrasonic Testing of Materials*, 1990.

3. **Auld B.A.** *Acoustic fields and waves in solids*, 1973.

4. **Schmerr L.W.** and **Sedov A.** (1989) An elastodynamic model for compressional and shear wave transducers, *Journal of Acoustic Society of America*, **86**, 1988–1999.

5. **Gridin D.** and **Fradkin L.J.** (1998) High-frequency asymptotic description of pulses radiated by a circular normal transducer into an elastic half-space, *Journal of Acoustical Society of America*, **104**, 3190-3198.

6. **Laturelle F. G.** (1990)The stresses produced in an elastic half-space by a normal step loading over a circular area, analytical and numerical results, *Wave Motion*, **12**, 107–127.

7. **Krishnamurthy C.V., Shankar M.** and **Krishnan Balasubramania** (2004) Patch Element Model for the Evaluation of Displacement Fields within an Elastic Solid from a Non-Contact Immersion Transducer: Application to the 2004 Ultrasonic Benchmark Problem, *Review of Quantitative Nondestructive Evaluation*.

8. **Ocheltree K.B.,** and **Frizzell L.A.** (1989) Sound Field Calculation for Rectangular Sources," *IEEE Transactions UFFC,* **36**, 242-248.

9. **Spies M.** (1994) Transducer-modeling in general transversely isotropic media via point-source-synthesis theory, *Journal of Non-destructive Evaluation,* 85–99.

10. **Adarsh K., Dewangan S., Rangan B.** and **Katragadda G.** (2003) Generic ultrasonic 3D ray tracing incorporating beam energy models, *Review of Progress in Quantitative Non Destructive Evaluation.*.